CERN – EUROPEAN ORGANIZATION FOR NUCLEAR RESEARCH

CLIC – Note – 1022

BEAM MOMENTUM CHANGES DUE TO DISCHARGES IN HIGH-GRADIENT ACCELERATOR STRUCTURES

Palaia, Andrea (Uppsala U.) ; Ziemann, Volker (dir.) ; Ruber, Roger (dir.) ; Ekelöf, Tord (dir.)

Abstract

The key questions left unanswered by the Standard Model, and the recent discovery of a Standard Model-like Higgs boson, demand an extension of the research on particle physics to the TeV energy scale. The Compact Linear Collider, CLIC, is a candidate project to achieve such goal. It is a linear lepton collider based on a novel two-beam acceleration scheme capable of high-gradient acceleration in X-band accelerator structures. The high electric fields required, however, entail the occurrence of vacuum discharges, or rf breakdowns, a phenomenon whose microscopic dynamics is not yet completely understood, and whose impact on the beam can lead to a severe degradation of the collider luminosity. The understanding of the physics of rf breakdowns has therefore become a significant issue in the design of a reliable accelerator based on CLIC technology. That is addressed experimentally through the study of accelerator structures performance during high-power operations. We report on such a study carried out on a CLIC prototype structure assembled in a resonant ring at SLAC. We characterise the experimental set-up through a complex least square analysis, and we show how breakdowns can be localised in the structure on the basis of rf measurements. The same methodology lays the ground for the study of the impact of rf breakdowns on the beam. We addressed that issue at the Two-beam Test Stand, an experimental area built within the CLIC Test Facility CTF3 at CERN, where we tested a CLIC prototype accelerator structure in the presence of an electron beam. There, we found that rf breakdowns can affect both the longitudinal and the transverse beam momentum, causing a reduction of accelerating gradient and transverse kicks to the beam trajectory. In view of the CLIC design, we finally discuss what is the impact of such effects on the collider luminosity, which can be drastically reduced.

Geneva, Switzerland
Date 14.12.2013

UPPSALA
UNIVERSITET

Digital Comprehensive Summaries of Uppsala Dissertations from the Faculty of Science and Technology 1096

Beam Momentum Changes due to Discharges in High-gradient Accelerator Structures

ANDREA PALAIA

CERN-THESIS-2013-227
12/12/2013

ACTA
UNIVERSITATIS
UPSALIENSIS
UPPSALA
2013

ISSN 1651-6214
ISBN 978-91-554-8802-4
urn:nbn:se:uu:diva-208567

Dissertation presented at Uppsala University to be publicly examined in Polhemsalen, Ångströmlaboratoriet, Lägerhyddsvägen 1, Uppsala, Thursday, 12 December 2013 at 10:15 for the degree of Doctor of Philosophy. The examination will be conducted in English. Faculty examiner: Bernhard Holzer (CERN).

Abstract

Palaia, A. 2013. Beam Momentum Changes due to Discharges in High-gradient Accelerator Structures. *Digital Comprehensive Summaries of Uppsala Dissertations from the Faculty of Science and Technology* 1096. 85 pp. Uppsala: Acta Universitatis Upsaliensis. ISBN 978-91-554-8802-4.

The key questions left unanswered by the Standard Model, and the recent discovery of a Standard Model-like Higgs boson, demand an extension of the research on particle physics to the TeV energy scale. The Compact Linear Collider, CLIC, is a candidate project to achieve such goal. It is a linear lepton collider based on a novel two-beam acceleration scheme capable of high-gradient acceleration in X-band accelerator structures. The high electric fields required, however, entail the occurrence of vacuum discharges, or rf breakdowns, a phenomenon whose microscopic dynamics is not yet completely understood, and whose impact on the beam can lead to a severe degradation of the collider luminosity.

The understanding of the physics of rf breakdowns has therefore become a significant issue in the design of a reliable accelerator based on CLIC technology. That is addressed experimentally through the study of accelerator structures performance during high-power operations. We report on such a study carried out on a CLIC prototype structure assembled in a resonant ring at SLAC. We characterise the experimental set-up through a complex least square analysis, and we show how breakdowns can be localised in the structure on the basis of rf measurements.

The same methodology lays the ground for the study of the impact of rf breakdowns on the beam. We addressed that issue at the Two-beam Test Stand, an experimental area built within the CLIC Test Facility CTF3 at CERN, where we tested a CLIC prototype accelerator structure in the presence of an electron beam. There, we found that rf breakdowns can affect both the longitudinal and the transverse beam momentum, causing a reduction of accelerating gradient and transverse kicks to the beam trajectory. In view of the CLIC design, we finally discuss what is the impact of such effects on the collider luminosity, which can be drastically reduced.

Andrea Palaia, Department of Physics and Astronomy, High Energy Physics, 516, Uppsala University, SE-751 20 Uppsala, Sweden.

ISSN 1651-6214
ISBN 978-91-554-8802-4
urn:nbn:se:uu:diva-208567 (http://urn.kb.se/resolve?urn=urn:nbn:se:uu:diva-208567)

List of papers

This thesis is based on the following papers, which are referred to in the text by their Roman numerals.

I A. Palaia, W. Farabolini, M. Jacewicz, R. Ruber and V. Ziemann. Effects of rf breakdown on the beam in the Compact Linear Collider prototype accelerator structure. *Phys. Rev. ST Accel. Beams*, 16:081004, Aug 2013.

II A. Palaia, V. Dolgashev, J. Lewandowski, S. Weathersby and V. Ziemann. High-gradient test of a X-band accelerator structure assembled in a klystron-driven resonant ring. *Submitted to Phys. Rev. ST Accel. Beams*, 2013.

III R. Ruber, V.Ziemann, T. Ekelöf, A. Palaia, W. Farabolini and R. Corsini. The CTF3 Two-beam Test Stand. *Nuclear Inst. and Methods in Physics Research, A*, 729:546-553 (2013).

IV W. Farabolini, F. Peauger, J. Barranco, S. Bettoni, B. Constance, R. Corsini, M. Csatari, S. Doebert, A. Dubrovskiy, T. Persson, G. Riddone, P. K. Skowroński, F. Tecker, D. Gudkov, A. Solodko, M. Jacewicz, T. Muranaka, R. Ruber, A. Palaia and V. Ziemann. Two Beam Test Stand Experiments in the CLEX CTF3 facility. In *Proceedings of IPAC2011, San Sebastián, Spain*, pages 29-31, 2011.

V A. Palaia. Commissioning of TBTS probe beam BPMs. *CTF3-NOTE-105*. (2013). *Submitted*.

Reprints were made with permission from the publishers.

List of other publications

The following publications are not included in this thesis.

VI V. Ziemann and A. Palaia. Luminosity loss due to kicks and mismatch from RF breakdown in a Linear Collider. *Manuscript.*

VII P. K. Skowroński, A. Andersson, J. Barranco, B. Constance, R. Corsini, S. Doebert, A. Dubrovskiy, F. Tecker, W. Farabolini, T. Persson, R. L. Lillestol, E. Ikarios, M. Jacewicz, A. Palaia and R. Ruber. Experimental Verification of the CLIC Two-Beam Acceleration Technology in CTF3. In *Proceedings of IPAC2013, Shanghai, China*, page 1436-1438, 2013.

VIII A. Palaia, M. Jacewicz, T. Muranaka, R.J.M.Y. Ruber and V.G. Ziemann. RF-breakdown kicks at the CTF3 Two-beam Test Stand. In *Proceedings of IPAC2012, New Orleans, Louisiana, USA*, pages 73-75, 2012.

IX M. Aicheler, P. Burrows, M. Draper, T. Garvey, P. Lebrun, K. Peach, N. Phinney, H. Schmickler, D. Schulte and N. Toge (Editors). A Multi-TeV Linear Collider Based on CLIC Technology: CLIC Conceptual Design Report. Technical Report *CERN-2012-007*, CERN, Nov 2012.

X A. Miyamoto, M. Stanitzki, H. Weerts and L. Linssen (Editors). Physics and Detectors at CLIC: CLIC Conceptual Design Report. Technical Report *CERN-2012-003*, CERN, Feb 2012.

XI P. K. Skowroński, J. Barranco, S. Bettoni, B. Constance, R. Corsini, M. Divall Csatari, A. E. Dabrowski, S. Doebert, A. Dubrovskiy, O. Kononenko, R. L. Lillestol, M. Olvegaard, T. Persson, A. Rabiller, F. Tecker, W. Farabolini, E. Adli, T. Muranaka, A. Palaia and R Ruber. The CLIC Feasibility Demonstration in CTF3. In *Proceedings of IPAC2011, San Sebastián, Spain*, pages 2042-1044, 2011.

XII D. Ogburn, A. Palaia, R. Ruber and V. Ziemann. Drive Beam Phase Measurement using RF data from the PETS. Technical Report *EuCARD-REP-2011-006*, CERN, 2011.

XIII A. Palaia, V. Dolgashev, J. Lewandowski and S. Weathersby. Diagnostics of RF Breakdowns in High-Gradient Accelerating Structures. In *Proceedings of DIPAC2011, Hamburg, Germany*, pages 527-529, 2011.

XIV W. Farabolini, D. Bogard, E. Chevallay, M. Csatari, A. Curtoni, P. Giradot, N. Lebas, F. Peauger, M. Petrarca, A. Palaia, R. Ruber, C. Simon and V. Ziemann. CTF3 Probe Beam LINAC Commissioning and Operations. In *Proceedings of Linear Accelerator Conference LINAC2010, Tsukuba, Japan*, pages 46-48, 2010.

Author's contribution to the papers

Paper I

I led the measurements also supervising the data acquisition during recurring visits at CERN. I developed the software used for the data acquisition and the data analysis, and I handled the writing of the paper. The interpretation of the experimental results is the outcome of a tight collaboration with the other authors.

Paper II

I participated in the data taking during a research visit at the Stanford National Acelerator Laboratory (SLAC). There, I learnt and implemented the analysis methods discussed in the paper, whose final form is a collaborative effort with the second author. The writing was handled by me.

Paper III

My contribution to this paper concerns the measurements of breakdown effects on the beam at the Two-beam Test Stand. Moreover, I participated in the experimental demonstration of the two-beam acceleration presented in the paper, and in the operation of the Two-beam Test Stand.

Paper IV

I participated in the commissioning and operation of the Two-beam Test Stand which are described in the paper. My original contribution concerns the measurements of breakdown effects on the beam, for which I contributed to the writing.

Paper V

I handled myself the data taking, analysis and writing of the paper. On the basis of my results, I contributed to improve the hardware with the help of others.

Contents

Acronyms

ASTA	Accelerator Structure Test Stand.
ATF	Accelerator Test Facility.
ATLAS	A Toroidal LHC Apparatus.
BPM	Beam Position Monitor.
CALIFES	Concept d'Accélérateurs Linéaire pour Faisceau Sonde.
CDR	Conceptual Design Report.
CERN	European Organization for Nuclear Research.
CLIC	Compact Linear Collider.
CMS	Compact Muon Solenoid.
CTF	CLIC Test Facility.
FEL	Free Electron Laser.
Fermilab	Fermi National Accelerator Laboratory.
ILC	International Linear Collider.
LEP	Large Electron-Positron Collider.
LHC	Large Hadron Collider.
LIL	LEP Injector Linac.
linac	linear accelerator.
PETS	Power Extraction and Transfer Structure.
rf	radio-frequency.
SLAC	Stanford National Acelerator Laboratory.
SPS	Super Proton Synchrotron.
TBL	Test Beam Line.
TBTS	Two-beam Test Stand.

1. Introduction

The topic of this thesis lies within the feasibility study of high-gradient acceleration of particle beams, in relation to the study of a high-energy and high-luminosity linear collider. More specifically, this thesis addresses the study of the effects of vacuum discharges occurring in accelerator structures on the accelerated beam and it is based on experimental observations carried out in the CLIC Test Facility 3 built at the European Organization for Nuclear Research (CERN).

Before coming to the heart of the matter, the physics motivations that drive the need of a high-energy linear collider, and the current proposals for such a machine, are outlined hereafter.

1.1 The Standard Model and beyond

Our current understanding of fundamental constituents of matter and of their interactions is described by the Standard Model [1–4], a quantum field theory that has proved to be valid over a wide range of energies and in a large number of stringent tests.

Because of the quantum nature of this theory, both the fundamental matter constituents and their interactions are described by particles, fermions of spin $\frac{1}{2}$ and bosons of spin 1, respectively.

Of the four fundamental forces that we know, only three fit into the Standard Model, namely the electromagnetic, the weak and the strong interaction. To this day, the Standard Model does not incorporate gravitation, because of the difficulties arising from a quantum formulation of general relativity. The fundamental particles described by the theory are twelve, six leptons and six quarks, which can be grouped into three doublets, so-called generations, according to their quantum numbers, or flavours. Why they are exactly three and not more or less is not explained by the theory. Up to now all these particles have shown no internal structure which is the reason why they are referred to as elementary particles. Finally, to each elementary particle corresponds an antiparticle, i.e. a particle with the same mass and opposite quantum numbers. Complex particles formed by combinations of a quark and antiquark or three quarks exists and are called hadrons.

Not all the fundamental particles are subject to the three interactions included in the theory. Only electrically charged particles, for instance,

are subject to the electromagnetic force, whose carrier is the photon. The quarks, on the other hand, are also subject to the strong interaction which is carried by eight gluons, whose number depends on the fact that quarks can exist in three different quantum states called colours. Finally, the weak interaction applies to all fundamental fermions with the peculiarity that electrically neutral leptons, called neutrinos, and quarks are subject to this force only when their flavours are mixed. This mixing mechanism is what explains, for instance, that a neutron can decay into a proton or that a neutrino can change its flavour through a process called oscillation. However, the amount of such mixing is not predicted by the theory and needs to be determined experimentally.

Despite the great success of the Standard Model, important questions remain unanswered and some of them cannot be explained within its framework. In addition to those already mentioned, there are other free parameters that cannot be derived within the basic principles of the theory and have to be experimentally measured. Among them, there are the masses of the elementary particles, which rise the more fundamental question of what is the origin of mass. In 1960s, Brout, Englert and Higgs approached to this problem and they independently formulated a mechanism which explains the mass of particles in terms of their coupling to a scalar field [5–7], a picture that resembles that of the coupling of charged particles to the electromagnetic field in terms of the electric charge. That model predicts that the interaction with such field is carried by a spin 0 boson, later named Higgs boson. The search for the Higgs boson has been since then one of the major goals in the attempt of completing the Standard Model picture.

The large number of free parameters and all the issues which cannot be explained within its principles, make the Standard Model an unsatisfactory theory [8]. However, other theories exists which extend the Standard Model to a higher energy scale and cope with its shortcomings, an example of which is the supersymmetry. In the context of these theories, dark matter, the asymmetry between matter and anti-matter, the possible existence of extra-dimensions and the unification of forces could find an explanation. Probing their validity is thus the main goal of the future research in particle physics.

1.2 Testing the Standard Model at particle colliders

Of all the members of the particle zoo described by the Standard Model, only a few are the building blocks of the matter at our energy scale. These are the electron and the two lightest quarks or more precisely, their combinations in stable hadrons like the proton and the neutron. All other heavier particles do not exist at our everyday energy scale

but can be produced in particle accelerators. There, beams of particles, typically electrons or protons which are easy to produce and store, are accelerated and impinged on a fixed target or against a second particle beam of the same or of a different species. The energy available in the centre-of-mass of the collisions is converted into other particles. Some of them are more long-lived than others and easier to observe, others are more elusive because they decay in a very short time and require meticulous experiments to be studied.

The search for particles predicted by the Standard Model has driven the construction of colliders capable of reaching higher and higher energies. Hadron collisions, typically proton-proton or proton-antiproton, although more difficult to study, are preferred in the search for particles whose mass is not precisely known. Protons, in fact, are not elementary particles, hence collisions actually occur between their constituents. The energy in the centre-of-mass of each collision varies from time to time and depends on the internal structure of the proton, through the so-called structure function. The collisions in which most of the energy of the colliding protons is actually involved and available in the centre-of-mass to create new particles are rare. More likely, the available energy is distributed among all the quarks that constitute the protons, which leads to collisions of quarks in a wide range of energies, and it also means that the number and variety of particles produced in each proton collision is large. Looking for a rare process in such a background is like looking for a needle in a haystack and it is not always an easy task.

Examples of fundamental discoveries achieved at hadron colliders are the observation of the electroweak force carriers, the $W^{\pm}$ and Z_0 bosons, in 1983 at the Super Proton Synchrotron (SPS) at CERN [9–11], subject of the 1984 Nobel prize in physics, and the more recent observation of the top quark at the Tevatron collider at the Fermi National Accelerator Laboratory (Fermilab) in 1999 [12].

In a lepton collider the number of particles produced in each collision is, in general, smaller than in a hadron collider. That is because leptons are elementary particles and their energy is fully available in the centre-of-mass of the collisions. Therefore discoveries at hadron colliders are typically followed by precision measurements at lepton colliders, where particle properties can be measured with a higher accuracy and resolution. That is the case, for instance, of the Large Electron-Positron Collider (LEP) built at CERN to follow up on the discoveries of the electroweak force carriers with precision measurements. There, the Standard Model was subject to stringent tests.

The search for the Higgs boson drove the design and construction of the Large Hadron Collider (LHC) at CERN, which aims at colliding protons at a centre-of-mass energy of 14 TeV. There, on 4 July 2012, the discovery of a particle with a mass between 125 and 127 GeV and

with properties similar to those of the Higgs boson was announced by the ATLAS and CMS collaborations [13, 14]. For the formulation of the mechanism confirmed by that discovery, Englert and Higgs have been awarded the 2013 Nobel prize in physics. Nevertheless, further statistics is needed to determine whether other Higgs bosons exist. Other theories, in fact, predict the existence of more than one Higgs boson, together with a whole new zoo of particles. Those theories aim at answering the questions left open by the Standard Model and it is to test their predictions that new colliders are needed.

1.3 Future linear particle colliders

All the research efforts in terms of designing future generation high-luminosity linear accelerators (linacs) carried out during the last decades, converged to two proposals: the International Linear Collider (ILC) [15] and the Compact Linear Collider (CLIC) [16]. Both are worldwide collaborations relying on different technologies capable of exploring different energy ranges. ILC is based on superconducting technology, well established and already largely used in massive accelerators and colliders such as LHC. Nevertheless, its maximum accelerating gradient is limited to 32 MV/m and it relies on klystrons as radio-frequency (rf) sources. That limits ILC to colliding electron and positron beams at a centre-of-mass energy of 500 GeV with the possibility to increase it up to an energy of 1 TeV. A higher collision energy would mean a significant increase in terms of length of the accelerator and number of klystrons required and is therefore not an option. CLIC, on the other hand, is based on normal-conducting technology which can provide an accelerating gradient of 100 MeV/m and therefore aims at colliding electron and positron beams at a centre-of-mass energy of 3 TeV. While ILC has recently published a technical design and implementation plan [17, 18], the CLIC design is still under study although its feasibility has recently been asserted with the publication of a Conceptual Design Report [16, 19].

In the context of this thesis, the feasibility study of the CLIC high-gradient acceleration is of particular interest. It requires high electric fields which entail the occurrence of violent discharges in the accelerator structures, known as vacuum discharges or rf breakdown, which can have severe effects on the accelerated beam resulting in a degradation of the collider performance. It is with the study of these effects and their impact on the CLIC design that this thesis is concerned.

1.4 Thesis structure

The remainder of this thesis is structured as follows.

Chapter 2 focuses on the description of the Compact Linear Collider according to its current design published in the Conceptual Design Report (Paper IX). This chapter introduces the context in which this thesis is situated and highlights the aspects relevant to the study that it addresses.

Chapter 3 describes the CLIC Test Facility at CERN which was built to address many of the feasibility issues identified in the CLIC design. This chapter focuses more specifically on the description of the Two-beam Test Stand, subject of Paper III, which is the experimental area dedicated to the study of the two-beam acceleration concept on which CLIC is based. There, the study of the effects on the beam of vacuum discharges in CLIC prototype accelerator structures has been addressed in the last years and it is the main topic of this thesis.

Chapter 4 describes the mechanism of vacuum discharges in high-gradient accelerator structures, their dynamics according to current models and the experimental observations that support such explanations.

Chapter 5 and 6 represent the core of the thesis and the author's original contributions. Chapter 5 contains a thorough description of the rf-based diagnostics of breakdowns carried out at the Stanford National Acelerator Laboratory (SLAC) on a CLIC prototype accelerator structure, which is also the subject of Paper II. Chapter 6 discusses the effects that breakdowns have on the beam on the basis of the measurements carried out at the Two-beam Test Stand. This is an important study for the feasibility demonstration of the CLIC two-beam acceleration concept and it is the topic of Paper I.

Finally, chapter 7 extends the results discussed in the previous chapter and discusses their relevance in the context of the design of the Compact Linear Collider.

In addition, basic concepts of beam physics and rf technology are recalled in Appendix A and B, respectively.

2. The Compact Linear Collider Study

At the beginning of the 1980s, everyone's eyes were on the CERN Super Proton Synchrotron (SPS) waiting for the imminent discovery of the weak force carriers [9, 10]. At the same time, the construction of the Large Electron-Positron Collider (LEP) [20], which was (and still is) the largest circular lepton collider ever built, had just been approved and the Large Hadron Collider (LHC) was just a study of a possible successor of LEP [21] which would have taken until 1994 to be formally approved [22]. Even then, CERN scientists already started considering the feasibility of new high-luminosity lepton colliders capable of exploring the TeV energy scale.

Particular attention was directed towards new concepts that could allow reaching high energies and high luminosity within a reasonable compactness and lower cost with respect to existing techniques [23]. A number of requirements was identified to be essential prerequisites for the design of such a machine, which included beam size in the micrometre or even nanometre range, small beam emittance, the need for a strong final focusing system and the overall necessity of a limited power consumption.

In 1985 an advisory panel was formed at CERN with the mandate of discussing new ideas for the realisation of a possible future CERN Linear Collider (CLIC) capable of accelerating electrons and positrons to the TeV energy scale.

A novel acceleration technique based on a two-beam scheme was proposed as an alternative to conventional acceleration methods [24]. It was based on the idea of producing rf power by passing an electron beam in a Free Electron Laser (FEL) section rather than using conventional rf sources, and to use such power to accelerate a second beam. An alternative to such scheme was proposed in 1987 which replaced the FEL section with a normal-conducting rf cavity in which the passage of a high-charge bunched beam produces rf power [25]. Such technique was identified as that on which the Compact Linear Collider (CLIC) study is based.

The CLIC study aims at developing a high-luminosity electron-positron linear collider capable of exploring the multi-TeV energy region. It is optimised for an energy of 3 TeV in the centre-of-mass of the collisions and for a luminosity of $2 \times 10^{34}\,\mathrm{cm}^{-2}\,\mathrm{s}^{-1}$. The two-beam acceleration scheme on which it is based has been optimised to achieve high accelerating gradients and efficient rf production. The proposed layout is shown in Fig. 2.1. It consists of two accelerator complexes called *main*

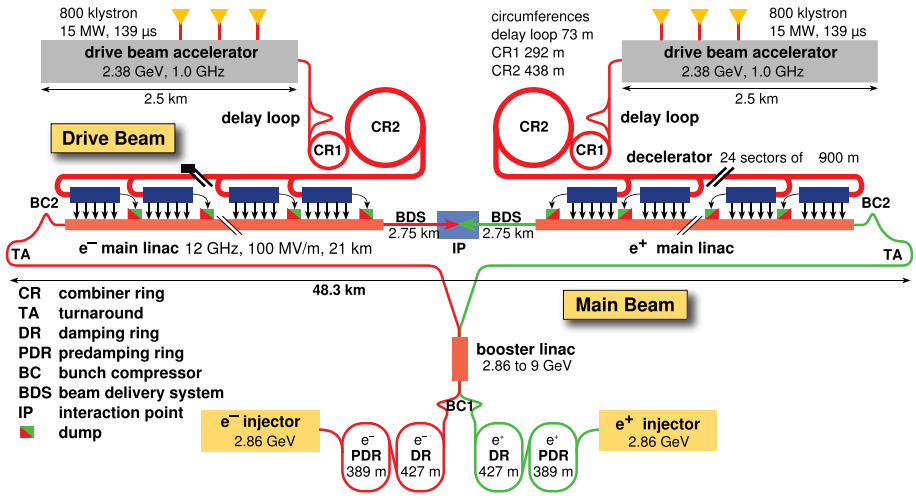

Figure 2.1: Layout of the Compact Linear Collider (CLIC) for collisions at an energy of 3 TeV in the centre-of-mass frame, according to the Conceptual Design Report. The drive beam complex shown at the top half of the figure is the rf power source for the main linac complex, shown at the at bottom half of the figure.

beam and *drive beam*, respectively shown at the bottom and at the top of Fig. 2.1. The main electron beam is generated at the bottom left of Fig. 2.1 and then accelerated to 2.86 GeV before being injected into two damping rings where the emittance is reduced. The bunch repetition frequency is then increased in a delay line and the beam energy brought to 9 GeV. Then the beam is transported to the main electron linac on the left of Fig. 2.1 where it is accelerated to an energy of 1.5 TeV. Finally, its transverse size is reduced to a nanometric scale and it is brought into collision with a positron beam of the same energy, which is generated in an almost identical complex. The main beams are accelerated in normal-conducting accelerator structures with a gradient of 100 MV/m. They are fed by multi-MW 12 GHz rf power obtained by the deceleration of a high-current beam, the drive beam, in resonant cavities called Power Extraction and Transfer Structures (PETSs), installed in a beam line that runs parallel with the main beam. In other words, the whole drive beam complex serves as rf power source for the main beam. Two drive beams are generated and accelerated to an energy of 2.38 GeV in two separate normal-conducting linacs at the top of Fig. 2.1. To maximise the power production, the temporal structure of the drive beam is such that the bunch spacing is as close as possible to the wavelength of the extracted 12 GHz rf power which corresponds to 2.5 cm. Such bunch structure is achieved in a delay loop and two combiner rings in which the beam frequency is increased by interlacing several bunch-trains.

Nowadays, the CLIC study is a joint global effort which involves 43 institutes and 22 countries. A Conceptual Design Report of a linear collider at the TeV scale based on CLIC technology was published by the CLIC collaboration in 2012 (Paper IX). It contains an extensive discussion of the physics and technology involved, together with a preliminary study of possible construction scenarios and an overall cost estimation of the project.

Here we briefly present the different parts of the drive beam and main beam complex and their critical points in terms of beam physics and technology, with particular emphasis on those issues, arising from the novel techniques used, which drove this thesis work.

2.1 Drive beam complex

The drive beam complex at the top of Fig. 2.1 is the rf power source for the CLIC main linac. It consists of two identical parts, each one providing the necessary power to accelerate respectively the electron and the positron main beams. Each part consists of a normal-conducting linac, a series of delay lines and rings called *recombination complex* in which the required temporal structure of the beam is obtained, and a *decelerator* in which rf power is produced by decelerating the beam at the expense of its energy.

Drive beam accelerator An electron beam is generated by a thermionic gun which produces 4.2 A, 142 µs long streams of electrons which are then bunched in travelling wave cavities (App. B) driven by 0.5 GHz rf. Because such frequency is half of that used to accelerate the beam, the bunching system is called *sub-harmonic* and it produces a train of electron bunches spaced by 2 ns or 60 cm, each one carrying a charge of 8.4 nC. In order to prepare the beam for the temporal structure subsequently achieved in the recombination complex, every 244 ns the phase of the sub-harmonic bunchers flips by 180° thus causing two consecutive buckets to be filled. That is repeated every 244 ns and it results in a temporal structure consisting of groups of 122 bunches occupying alternatively only even or odd buckets, as schematically shown in Fig. 2.2. The beam is said to be phase-coded. Afterwards the beam is first accelerated from about 140 keV to 50 MeV and then further accelerated to the final energy of 2.4 GeV. To optimise the amount of rf power used, only the exact amount of power actually spent to accelerate the beam is fed to each accelerator structure. The structure is therefore said to be fully-loaded by the beam.

Specific attention is paid to the design of the low energy part of the injector to limit the growth of the beam emittance, which is induced by

the strong space-charge forces caused by the large bunch charge. That is achieved by careful simulations of the space-charge effects and optimisation of the focusing system. An additional issue are satellite bunches, i.e. unwanted particles that occupy the space between two consecutive bunches thus reducing the efficiency of power transfer to the beam and increasing the chances of activation of the hardware in case they are lost. That is addressed by a cleaning system that makes use of fast rf kickers to send unwanted satellites towards a beam dump.

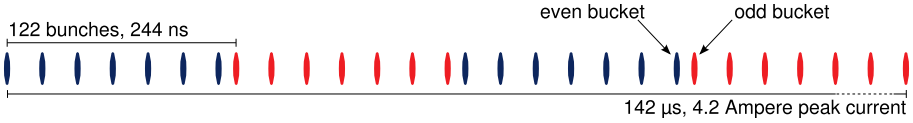

Figure 2.2: Phase-coding in the drive beam sub-harmonic bunching system.

Recombination complex In the recombination complex the length of the bunch-train is reduced and the bunch repetition frequency is increased. It consists of a delay line called *delay loop* and two rings called *combiner rings* in which the final bunch-train structure of 24 sub-trains of bunches repeated at a frequency of 12 GHz is achieved.
When the phase-coded beam shown in Fig. 2.2 reaches the delay loop, a 0.5 GHz rf deflector kicks every even bucket in the delay loop and lets every odd bucket continue on the straight path, as sketched in Fig. 2.3a. The length of the delay line is such that the time of flight of the electrons along it is exactly 244 ns. At the exit of the delay loop the bunches are kicked by another rf deflector back onto the straight path such that they interleave with the ones that where not kicked in the delay loop. The temporal structure of the bunch-train after the delay loop consists of 244 ns long sub-trains of bunches repeated at a frequency of 1 GHz, as sketched in Fig. 2.3b.
At this point, three bunch-trains like the ones shown in Fig. 2.3b are injected in the first combiner ring and interleaved with each other such that the bunch repetition rate is increased to 3 GHz. That is achieved by tuning the length of the ring in such a way that after one turn, a bunch-train is 60° out of phase later than the bunch-train injected at that moment.
In the same fashion, four sub-trains coming out of the first combiner ring are injected in the second combiner ring, where they are interleaved in such a way that at the end of the fourth turn the bunch repetition frequency is increased to 12 GHz and the bunch-train length is still 244 ns and spaced from the preceding and following bunch-trains by about 5.6 µs.

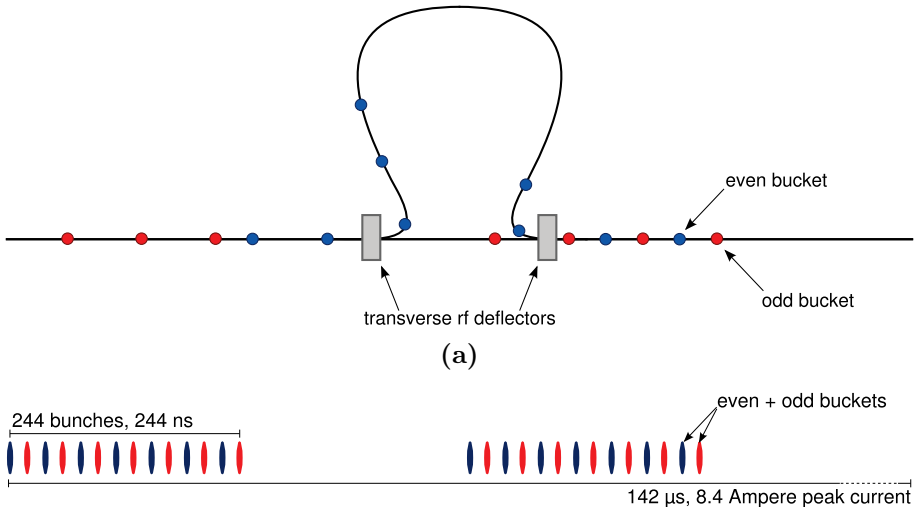

Figure 2.3: Sketch of (a) the bunch frequency multiplication technique in the delay loop and (b) temporal structure of a bunch-train after the delay loop.

Decelerator The decelerator is the rf power source for the main linac. It runs parallel to the main linac and it is divided in 24 sectors in each one of which a 101 A, 2.4 GeV and 244 ns long bunch-train is decelerated and its energy converted to rf power. The deceleration occurs in travelling wave room temperature resonant cavities called Power Extraction and Transfer Structure (PETS) where each and every bunch sees the maximum decelerating wakefield excited in the cavity by the preceding bunch. The process continues for all the bunches in the bunch-train until a steady state of maximum deceleration is reached. Each PETS produces a 244 ns long pulse of 135 MW which is transferred to the main beam accelerator structures. Each bunch-train is decelerated in 1492 PETS over a length of about 1 km until it reaches the final energy of 240 MeV.

Dump lines Although about 90% of the drive beam kinetic energy is converted to rf power, the spent beam still has to be dumped. The average power to dump is 0.54×10^6 W per pulse with a repetition rate of 50 Hz (0.54×10^6 kW). Although no definite specification for a beam dump exists, a water absorber has been proposed which is about 1.5 m long and in which the water flow has a vertical velocity of $3\,\mathrm{mm\,s^{-1}}$ to efficiently dissipate the heat.

2.2 Main beam complex

The main beam complex at the bottom of Fig. 2.1 is the part of CLIC in which positron and electron beams are generated, accelerated and brought into collision. The rf power source for the main linac is the drive beam complex, described above.

Injectors Two separate injectors for electrons and positrons have been designed for the main beam accelerator complex, as shown at the bottom of Fig. 2.1. The baseline configuration provides for polarised electrons and unpolarised positrons, although a polarised positron source is considered as an option for future upgrades. Both injectors have a similar design consisting of a particle source followed by a pre-acceleration stage and a normal-conducting linac. Polarised electrons are extracted from a photocathode excited by a polarised laser beam which produces a 312 ns long train of electrons which are bunched in a 1 GHz bunching system and then pre-accelerated to 0.2 GeV. The unpolarised positron source is based on a separate 5 GeV unpolarised electron beam sent onto a crystal tungsten target where soft photons are produced and in turn sent onto an amorphous tungsten target where positrons are produced in electromagnetic showers. They are then pre-accelerated to 0.2 GeV and subsequently sent to the linac which accelerates positrons and electrons to an energy of 2.86 GeV before the injection in the damping rings.

Damping rings The main purpose of the damping rings is to cool both electron and positron beams by emission of synchrotron radiation to reach the ultra-low emittance required for the injection in the main linacs which bring them into collision. One pre-damping ring followed by one damping ring is built for each species of particles. Afterwards both electron and positron beams are injected in a delay loop in which the bunch repetition frequency is doubled to 2 GHz.

Ring to Main Linac Transport At the exit of the damping rings the beam is transported for about 27 km from the ground level to the main linac which is located 100 m underground. Meanwhile, it is accelerated in the booster linac in the middle of Fig. 2.1 to the main linac injection energy of 9 GeV.

Main linac The main linac is where the two-beam acceleration actually takes place. It consists of two laser-straight 21 km long linacs in which electrons and positrons are accelerated from the injection energy of 9 GeV to the collision energy of 1.5 TeV. Each linac is equipped with about 71 thousand 12 GHz travelling wave accelerator structures in which the beam is accelerated with a gradient of 100 MV/m. Drive beam PETS and main beam accelerator structures are assembled together in so-called

CLIC modules which differ according to which part of the linac they are installed in, but in general each PETS powers two accelerator structures. One of the main issues in this part of the complex is the preservation of the ultra-low emittance during the beam acceleration and transport to the collision point. Another challenge in the main linac is the stable operation of the accelerator structures. The extremely high accelerating gradient of 100 MV/m in fact entails the presence of strong electric fields which can randomly trigger discharges in the accelerator structures, so-called rf breakdown. Those are a severe problem for the operation of any accelerator and in particular for CLIC, where they can severely degrade the luminosity. For this reason, assuming that a breakdown causes a bunch-train to fully miss the collision, the maximum tolerated breakdown rate in CLIC is set to 3×10^7 per pulse per metre, which corresponds to 1% of lost pulses.
The feasibility of stable operation of high-gradient accelerator structure is the object of extensive research efforts. This thesis focuses on the effect that rf breakdown have on the beam accelerated in CLIC prototype structures, which is the subject of Paper I.

Beam delivery system At the end of the main linac the beam is transported to the collision point through a 2750 m long beam line, as sketched in the middle of Fig. 2.1. The strong optics used in this part of the collider is called final focusing and it is used to make the transverse beam size as low as 45 nm on the horizontal plane and 1 nm on the vertical plane at the collision point. Electron and positron beams collide with an angle of 20 mrad so that afterwards they can be extracted in the forward direction without interfering with the incoming beams. Crab-cavities are used to rotate the bunches in the horizontal plane for head-on collisions in order not to loose luminosity due to the crossing angle.

Post collision line Every time that electron and positron bunches cross in the collision point only a small fraction of particles does really interact while all the others continue straight. The transverse size of the uncollided beams is basically unchanged whereas that of the collided beams is bigger and the post collision line is designed to accept both beams and transport them to the beam dump.

Each one of the subsystems of both the drive beam and the main beam complex address physical and technological issues whose feasibility demonstration is a preliminary step towards the realisation of a linear collider based on CLIC technology. More specifically, four areas have been identified as the most critical for its design, which are [16]:

- achievement of an accelerating gradient of 100 MV/m in the main linac, that addresses also the study of vacuum discharges in accelerator structures and their effect on the beam, which is the subject of this thesis;
- generation of a high-current drive beam, production of rf power through stable drive beam deceleration and use of such power to efficiently accelerate the main beam;
- generation and preservation of an ultra-low emittance main beam which has to be aligned with unprecedented accuracy through active magnet stabilisation against mechanical vibrations;
- machine protection against failures together with a high machine availability.

The feasibility of ultra-low emittance beams has been demonstrated for a vertical emittance even beyond the CLIC target at the Accelerator Test Facility (ATF) in Japan [26] and at the Swiss FEL [27], whereas horizontal emittances comparable to the CLIC target are aimed at MAX-IV in Sweden [28] and at PEP-X in USA [29], two synchrotron radiation light sources currently under construction. The achievement of high-gradient acceleration and the issues related to the drive beam represent the scientific goals that drove the construction of a CLIC Test Facility, which is addressed in the next chapter.

Table 2.1: Summary of CLIC parameters. Emittances are normalised.

Drive beam	
charge per bunch	8.4 nC
electrons per bunch	5.25×10^{10}
bunch spacing	2.5 cm or 83 ps
bunch-train length	244 ns
number of bunches per bunch-train	2922
bunch-train current	100 A
number of bunch-trains per macro-bunch	24
macro-bunch length	142 µs
average current	4.2 A
emittance before deceleration	1.5 µm rad
energy before/after deceleration	2.37 GeV/0.24 GeV
repetition rate	50 Hz
power production per PETS	135 MW
Main beam	
charge per bunch	0.6 nC
electrons per bunch	3.7×10^9
bunch spacing	15 cm or 0.5 ns
bunch-train length	156 ns
number of bunches per bunch-train	312
bunch-train current	1.2 A
emittance horizontal/vertical at injection	≤ 600 nm rad/≤ 10 nm rad
emittance horizontal/vertical at collision	≤ 660 nm rad/≤ 20 nm rad
energy injection/collision	9 GeV/1.5 TeV
repetition rate	50 Hz

3. The CLIC Test Facility

An extensive experimental programme aimed at testing the feasibility of the CLIC technology started at CERN during the late 1980s, with the construction of a CLIC Test Facility (CTF) [30]. Its five-year long experimental programme ended in 1995 and led to the first successful test of rf power production by deceleration of a high-charge drive beam in a 30 GHz normal-conducting accelerator structure. Moreover, the acceleration of the same beam with a maximum gradient of 94 MV/m in a second identical structure fed with the power extracted in the first place, was also demonstrated. In accordance with the CLIC design at that time, the drive beam was generated in a laser-driven photocathode. The CLIC experimental programme then continued in a second facility called CLIC Test Facility (CTF)II where the two-beam acceleration scheme was actually tested with two distinct electron beams, a drive beam and a so-called probe beam which mimicked the CLIC main beam. This time the drive beam was decelerated in specifically designed structures called Power Extraction and Transfer Structure (PETS) and the rf power produced was used to accelerate a low-charge single-bunch probe beam [31].

Meanwhile, the CLIC design evolved and a new facility called CTF3 was proposed in 1999 [32] to address the five following key feasibility points [33]:

- test of high-gradient accelerator structures with wakefield damping features;
- generation of a drive beam in a fully loaded linac;
- design and test of a Power Extraction and Transfer Structure with the capability of being switched on and off;
- validation of beam stability and losses in the drive beam decelerator;
- test of a CLIC module.

The first three points have been demonstrated at CTF3 whereas the fourth is still under study and the last is planned in the near future. More specifically, a Test Beam Line (TBL) [34] equipped with 16 PETS is dedicated to the study of the drive beam deceleration and an additional experimental area called Two-beam Test Stand (TBTS) together with an accelerator which provides a multi-bunch probe beam is entirely dedicated to two-beam acceleration studies. There, the problem of vacuum discharges, or breakdowns, that represent the main limitation to the stable operation of a high-gradient accelerator structure, is addressed. It

Table 3.1: Comparison of CTF3 and CLIC parameters.

	CLIC	**CTF3 2012**
Drive beam		
current	100 A	28 A
energy	2.38 GeV	150 MeV
bunch frequency	12 GHz	12 GHz
Main/Probe beam		
current	1 A	0.2 A
energy	9 GeV	180 MeV
bunch frequency	2 GHz	1.5 GHz
bunch charge	> 0.6 nC	0.085 - 0.6 nC
bunches per pulse	312	1 - 225
repetition rate	50 Hz	0.8 - 5 Hz
transverse emittance	< 0.6 mm mrad	8 mm mrad

is with the study of such phenomena and the effects that they have on the beam that this thesis is concerned.

To reduce the cost of the installation, the parameters of CTF3 differ from those proposed for CLIC as summarised in Table 3.1. The main difference is the base frequency of the drive beam accelerator which is 3 GHz as opposed to the CLIC main linac frequency of 1 GHz, in order to re-use all the rf components, klystrons, modulators, compressor cavities and waveguides previously installed in the LEP Injector Linac (LIL) complex. Such choice affects the maximum achievable beam energy which is about one tenth of the CLIC drive beam energy for a beam current of about 4 A. A second important difference is the presence of only one combiner ring, because the second implements the same bunch interlacing technique implemented by the first, and it is therefore not considered essential in this feasibility demonstration phase. Finally, the overall length of the drive beam linac, the decelerator and the probe beam linac are much shorter than in CLIC.

A thorough description of CTF3 and of the status of the experimental verification of the CLIC technology is documented, among others, in Paper XIV, XI, VII and IV. Additionally, Paper III contains a thorough description of the layout and commissioning of the Two-beam Test Stand. In light of that, the brief description of CTF3 that follows is meant to introduce the experimental context in which the study addressed by this thesis was carried out.

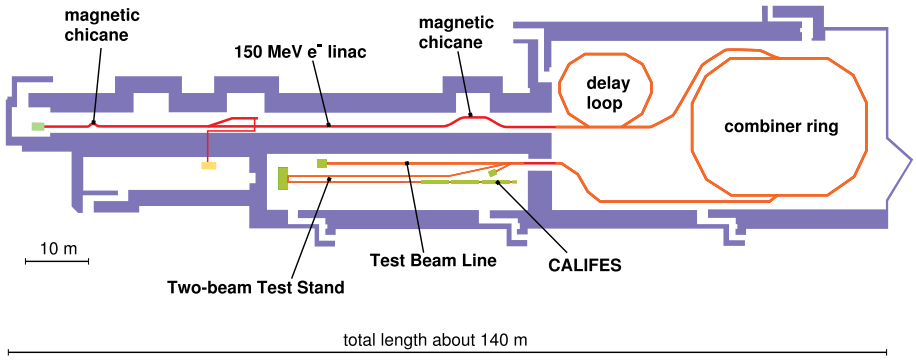

Figure 3.1: Layout of the CLIC Test Facility 3 at CERN.

3.1 Drive beam

The CTF3 drive beam complex consists of a normal-conducting electron linac followed by a magnetic stretching chicane, a delay loop and a combiner ring.

A 4 A, 1.5 µs long train of electron bunches is produced in a thermionic gun pulsed at a frequency of 3 GHz. It is then compressed in a magnetic chicane where off-energy electrons are stopped by collimation slits, and accelerated in a S-band linac to about 150 MeV. Afterwards, the bunch length can be manipulated in a stretching magnetic chicane where it can be adjusted to prevent excitation of coherent synchrotron radiation downstream in the beam line.

At the beginning of the linac, the bunch frequency is reduced to 1.5 GHz and coded with phase shifts of 180° every 140 ns in order to obtain sub-trains that can be interleaved two by two by passing one of them in the delay loop. There the bunch frequency is increased again to 3 GHz and the peak current is about 8 A. Four of these 140 ns long bunch-trains are then sent in the combiner ring where their bunch frequency is increased to 12 GHz and the peak current reaches 28 A. This mode of operation is referred to as factor 8 recombination.

Alternatively, the delay loop can be bypassed thus making the subharmonic bunching also unnecessary. In that case, four bunch-trains can be transported and injected directly in the combiner ring, where they are interleaved with each other in a 140 ns long bunch-train with bunch repetition frequency of 12 GHz and peak current of 16 A. This mode of operation is referred to as factor 4 recombination. Finally, in case the combiner ring is also bypassed, the beam is referred to as uncombined.

The drive beam is eventually transported to an experimental area and injected into a Test Beam Line (TBL) designed to provide a test bed for the CLIC drive beam decelerator, or in the Two-beam Test Stand

(TBTS), designed to demonstrate the feasibility of the two-beam acceleration concept.

3.2 Probe beam

The CLIC main beam linac is mimicked in CTF3 by the CALIFES (Concept d'Accélérateurs Linéaire pour Faisceau Sonde) linac that provides the so-called probe beam which is injected into the TBTS for two-beam acceleration experiments. A detailed description of its design can be found in [35]. It consists of a laser-driven photo-injector and a linac based on two 4.5 m long 3 GHz travelling-wave structures. A third structure installed right after the photocathode and identical to the other can be used as a buncher.

The beam line is equipped with beam profile monitors, re-entrant cavity beam position monitors for orbit measurements and ends with a spectrometer line for beam energy measurements.

The temporal structure of the beam is defined by the laser that drives the photo-injector, which consists of trains of 1 ps long ultra-violet light pulses emitted with a frequency of 1.5 GHz. Macro-pulses of 1 to about 300 pulses can be produced which are transported for about 80 m to the photo-cathode. There, electron bunches are generated and accelerated in the linac up to a maximum energy of about 200 MeV measured with 1% accuracy.

The maximum charge that can be accelerated in a bunch-train is 19 nC. Such limit is set by the accelerator structures which, because of cost reasons, were not specifically developed for the probe beam but re-used from the LEP Injector Linac complex.

3.3 Two-beam Test Stand

The Two-beam Test Stand was built to test the CLIC two-beam acceleration scheme, more specifically to test the operation of Power Extraction and Transfer Structure (PETS), to study the effects of breakdown on drive beam and probe beam and to test the operation of a full CLIC module [36]. Its design and commissioning is thoroughly discussed in Paper III and it is summarised hereafter. As sketched in Fig. 3.2, it consists of two parallel beam lines designed to test the power extraction from the CTF3 drive beam in a CLIC prototype PETS. Such power is then fed to a CLIC prototype accelerator structure in which the CTF3 probe beam is accelerated with a nominal gradient of 100 MeV/m. Both beam lines consist of a 11 m long straight section and end with a 1.6 m long spectrometer line where the beam energy is measured before the

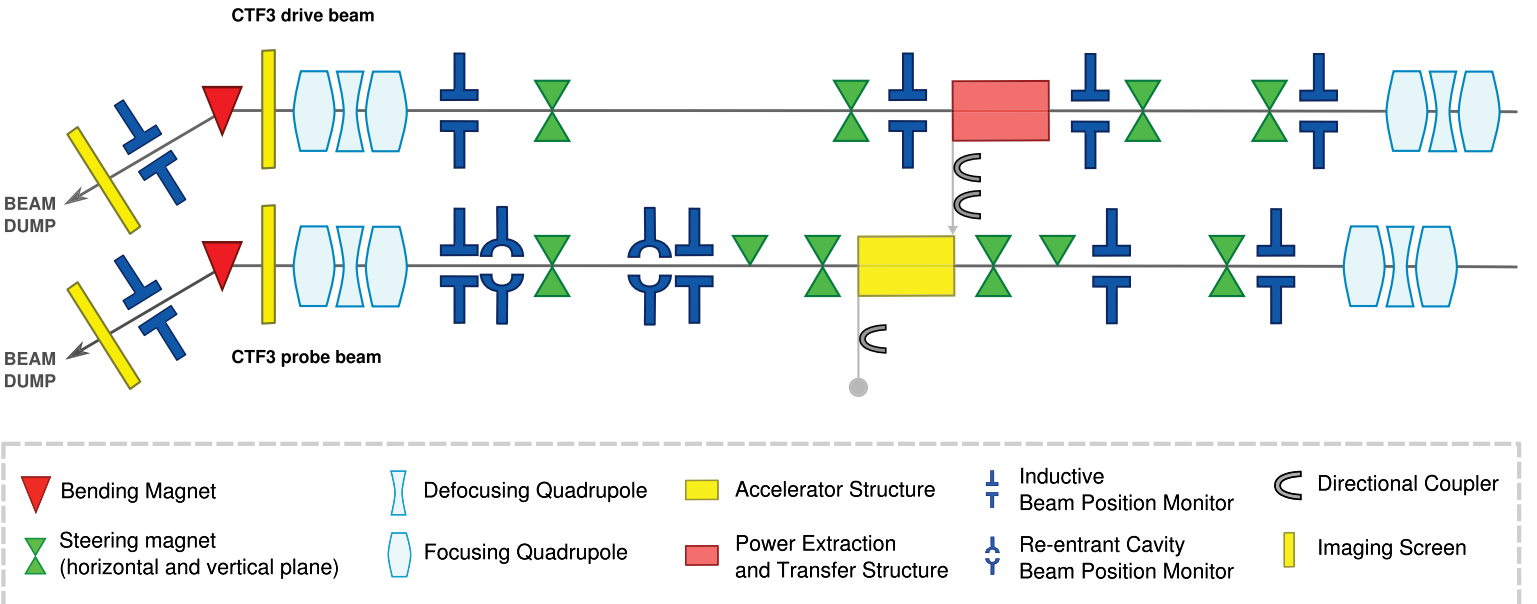

Figure 3.2: Layout of the Two-beam Test Stand. The drive beam is injected from the right in the beam line at the top half of the figure and it is decelerated in a Power Extraction and Transfer Structure. The probe beam is injected from the right in the beam line at the top botton of the figure, and it is accelerated in a CLIC prototype structure fed with the power extracted from the drive beam. Both beam lines are equipped with beam and rf diagnostics and end with a spectrometer line where the beam energy can be measured.

beam dump. Both beam lines are equipped with five inductive Beam Position Monitors (BPMs) [37], two upstream and three downstream of each structure, the last one of which is localised in the spectrometer line. The probe beam line sketched at the bottom of Fig. 3.2 is also equipped with two cavity BPM [38] downstream of the accelerator structure. They were installed at a later stage to resolve fast changes in the beam position thanks to their bandwidth of 600 MHz centred at a frequency of 6 GHz which makes them insensitive to the low frequency noise visible on the inductive BPM signals.

Both beam lines are equipped with removable imaging screens which are used to measure the beam profile either just before or after the dipole magnet which bends the beam in the spectrometer line. The screen in the spectrometer line of the probe beam is a high sensitivity fluorescent screen whereas at the end of the straight section of the beam line, before the spectrometer, both an optical transition radiation screen and a scintillating screen [39] are available.

The accelerator structure installed in the beam line is the CLIC prototype `TD24_vg1.8_disk` [40]. A cross-sectional view of its 3D model is shown in Fig. 3.3. It is a 12 GHz travelling-wave resonant structure

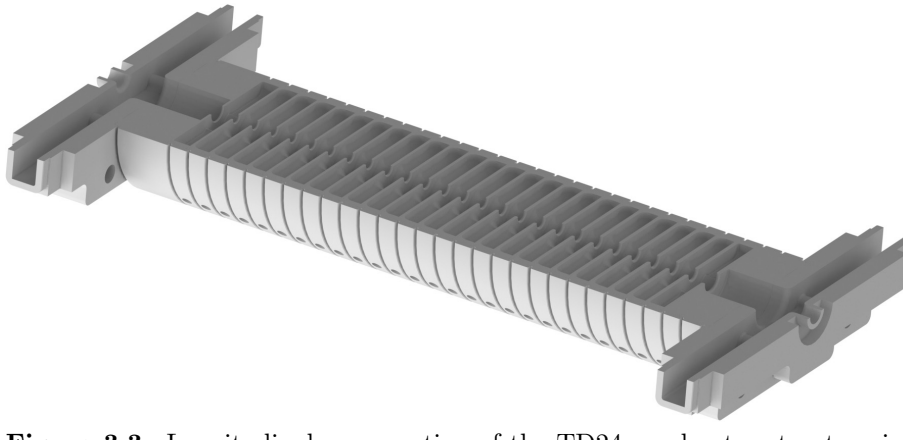

Figure 3.3: Longitudinal cross-section of the TD24 accelerator structure installed in the Two-beam Test Stand. The structure consists of 24 cells plus a matching cell and a double-feed coupler at the input and output ports.

made of copper, with longitudinal tapering and no high-order modes damping features. It has 24 regular cells and two additional matching cells at each end. It is equipped with directional couplers at its input and output ports. Their output signals are sent to diode detectors and in-phase and quadrature demodulators, and then calibrated for power and phase measurements. Such diagnostics has some problematic aspects such as, for instance, the limited dynamic range of the diode detectors, which makes their calibration difficult and sometimes not reliable. An

alternative approach to the measurement of power level and phase is thoroughly discussed in Chapter 5 and is the subject of Paper II. An example of rf signals measured during a breakdown in the accelerator structure is shown in Fig. 3.4. Paper II.

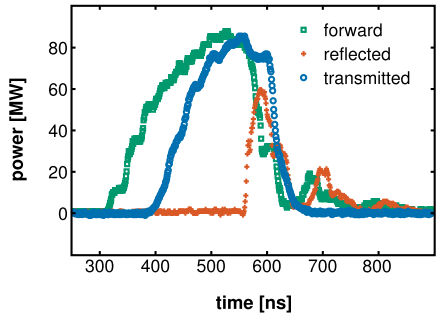

Figure 3.4: Measurements of rf power in case of breakdown in the accelerator structure. The power fed to the structure (green signal) is measured in the input coupler and then again in the output coupler (blue signal) where it arrives with a delay of about 65 ns, which is the filling time of the structure. A breakdown occurring during the rf pulse causes a fraction of the power to be reflected (red signal) backwards, towards the input coupler, where it is measured. Accordingly, the transmitted power drops abruptly to zero.

3.3.1 Two-beam acceleration

The demonstration of the feasibility of a Two-beam Acceleration scheme for CLIC is the main reason for the construction of the Two-beam Test Stand. There, the two-beam acceleration was successfully tested for the first time on 5 August 2010. The effect of the acceleration is visible in Fig. 3.5, which shows a measurement of the beam energy at the end of the spectrometer line taken while the rf phase in the accelerator structure was changed. To obtain the maximum acceleration the arrival time of the probe beam bunches in the accelerator structure must be synchronised with the maximum of the 12 GHz accelerating field. That is achieved by slowly varying the probe beam 3 GHz phase until the maximum acceleration is measured.

Most of the work collected in this thesis focuses on the study of the effects of rf breakdown on the probe beam, an example of which is shown in Fig. 3.6. The two spots visible there belong to the same beam pulse, and are caused by transfer of transverse momentum to the beam during an rf breakdown. Hence the beam trajectory of the later part of the bunch-train is shifted, or kicked, in the transverse plane and it results in two distinct beam spots. A thorough discussion of that observation can be found in Chapter 6 and is published in Paper I.

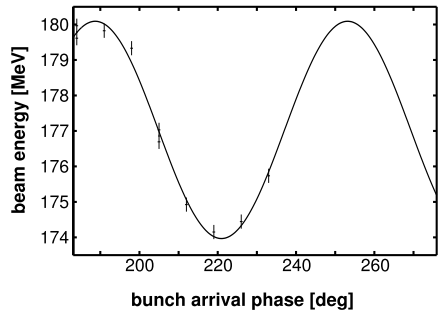

Figure 3.5: Probe beam energy measurements taken while changing the arrival phase of the probe beam bunches in the accelerator structure.

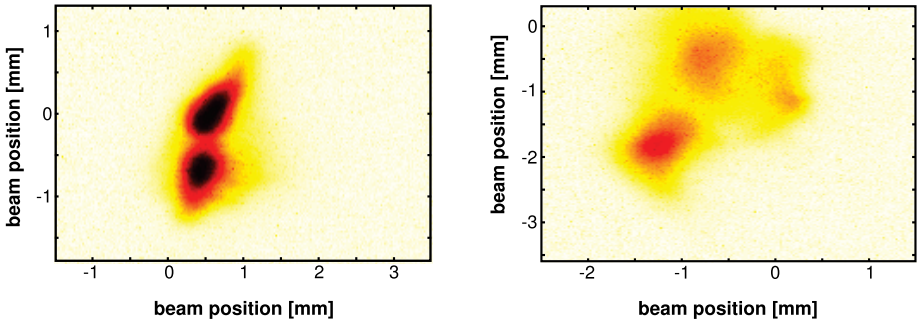

(a) **(b)**

Figure 3.6: Effects of breakdown on the beam. Beam profile measurement showing a double beam spot in presence of rf breakdown in the accelerator structure.

Before getting to the heart of the discussion of the effects of rf breakdown on the beam, it is worth presenting the broad field of vacuum discharges, of which rf breakdowns in accelerator structures are a particular case. Experimental observations and theoretical models on which our current understanding of such phenomena is based, are discussed in the next chapter.

4. Vacuum discharges

Vacuum discharges, also called arcing, or breakdown, represent the main limitation to the reliable operation of high-gradient accelerator structures. Vacuum discharges are well known for about one century, and they have their physical basis in electron field emission, which was theoretically explained by quantum tunnelling of electrons in the late 1920s by Fowler and Nordheim. Since the 1980s vacuum discharges have become one of the main R&D topics in the field of particle accelerators because of the design of high-energy colliders based on room temperature acceleration technology, where the electromagnetic fields are so high that they can initiate field emission which randomly turns into an avalanche process called rf breakdown.

This chapter goes through the experimental observations carried out over more than one century on which the current understanding of breakdown physics is based.

4.1 Historical theoretical background

The first scientific investigations on breakdown or arcing phenomena in regions of very high electric field date back to 1897 when it was observed that even prior to breakdown a vacuum gap had a finite conductivity due to a so-called pre-breakdown current, the magnitude of which was proportional to the gap voltage. It was not until 1920 that such current was identified as an electron current originating from a cold emission process [41].

It was subsequently obvious to look for an interpretation of such phenomenon in terms of the theory of field emission from a metal surface proposed by Fowler and Nordheim in 1928 and based on the quantum tunnelling of electrons [42]. That was not sufficient, however, to predict the magnitude of the currents experimentally observed, since it would have required field strengths of the order of GV/m on the basis of the Fowler-Nordheim theory. Therefore, the concept of field enhancement was proposed to explain how such field strength could be reached. That was based on the idea that microprotrusions on the surface of an electrode cause locally enhancement of the applied electric field thus increasing the probability of electron emission by tunnelling effect. The magnitude of the field emission current is dependent on the shape of the

emitter through a so-called field enhancement factor and on the minimum energy needed to extract one electron from the electrode surface through the work function [43, Chapter 18].

Several experiments were conducted to investigate the dependence of the breakdown voltage on macroscopic parameters of the gap, like the electrode material, production and cleaning procedure and the gap width. It was observed, for instance, that a 0.5 mm gap can sustain 20 kV whereas a 100 mm gap does not sustain more than 1 MV as opposed to the multi-megavolt regime that would be expected. Another important result was the observation that electrode material was transported across the gap and irrespective from which electrode, suggesting that some other processes common to both electrodes and other than the field emission were involved.

In the mid of the 1960s it was recognised that the electrons extracted through field emission from microprotrusions on the cathode surface can bombard the anode surface and create hot-spots where, in case they have enough power, the electrode is locally vaporised releasing enough material to trigger a breakdown in the gap. This mechanism is called *anode-initiated*, as opposed to the *cathode-initiated* one in which the microprotrusions themselves become unstable and start emitting the material that triggers the breakdown. The dependence of these two mechanisms on the microprotrusion geometry was also understood: a sharp geometry leads to a cathode-initiated breakdown whereas a more blunt geometry leads to an anode-initiated one.

It is worth noting that other processes have to be taken into account to describe the dynamic of breakdowns in a vacuum gap. For example, impurities and contaminants, as well as microscopic damages on the electrode surfaces, are sources of microprotusions. Moreover, intrusive material and gas desorption from the surfaces of the gap can degrade the vacuum and increase the probability of breakdown. For these reasons, the entire manufacturing process, the electrode surface preparation procedure and its operational history turn out to be crucial issues for reliable operation of a high-voltage vacuum gap.

To summarise, the breakdown process consists of three main phases [44], as sketched in Fig. 4.1. First, a so-called *onset* phase when the field emission current flowing through microprotrusions causes ohmic heating such that evaporation of neutrals into vacuum starts and is immediately followed by their ionisation caused by the same field emission current. This phase lasts for about 1 ns and is followed by a so-called *burning* phase which consists of the formation of a plasma sheath above the field emitter. As a result the local field is further enhanced up to 10 GV/m which leads to the melting of the emitter tip and sputtering of ions and neutrals from the surface into the plasma. Finally, the sputtering process creates new emitters which, in turn, start feeding the plasma and new craters

form on the surface. This phase is called *cratering* and it continues as long as there is power available to feed the field emission. Afterwards, the plasma is expected to disappear by expansion or recombination.

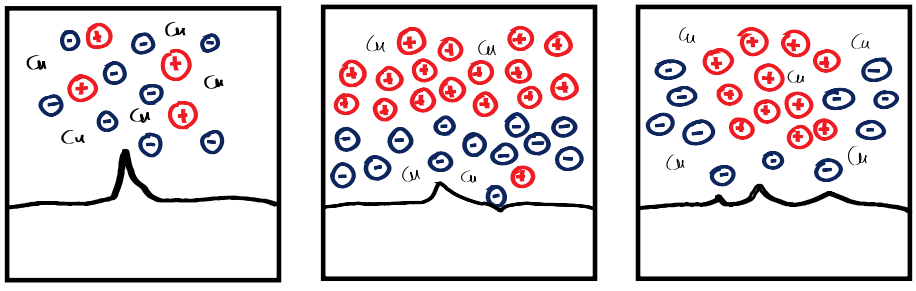

Figure 4.1: Phases of a breakdown. From the left, the *onset* starts with field emission from a microprotrusion which heats the emitter with consequence evaporation of neutrals and their immediate ionisation. In the middle, the *burning* phase in which the plasma growth into a plasma sheath and the field on the emitter is further enhanced. The last phase on the right is the *cratering* phase and is characterised by sputtering on the surface which produces craters and protrusions that can turn into new field emitters. This phase goes on until the field emission is not sustained anymore by external power flow and the plasma disappears.

During the last decades, many experimental techniques have been used to investigate microscopic and macroscopic aspects of vacuum arcs. Among them, test of different electrodes under static or rf fields and imaging of electrode surfaces in scanning electron microscopes before and after high-gradient testing. An example is given in Fig. 4.2.

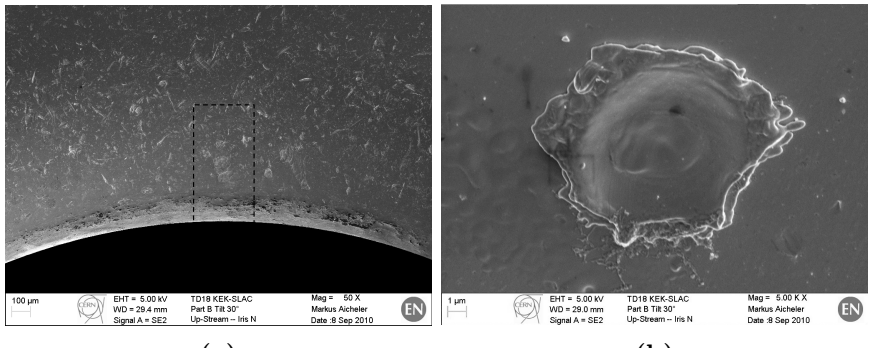

(a) **(b)**

Figure 4.2: Damages caused by breakdowns in a CLIC prototype accelerator, observed in a scanning electron microscope. (a) The dashed area on the iris of one of the disks of the structure is further magnified in (b) to show a crater cased by a breakdown. Images courtesy of Markus Aicheler, CERN.

The analyses of data from high-gradient testing of accelerator structures show a strong correlation between the accelerating field gradient E, the rf pulse length τ_p and the breakdown rate BDR [45]:

$$BDR \propto E^{30}\tau_p^5 \tag{4.1}$$

This scaling law has been largely used as guidance in the rf design of accelerator structures. Nevertheless, recently new criteria has been suggested which are based on the concept of power flow in the structure and local pulsed heating of a breakdown site [46].

The design efforts of a high-gradient X-band accelerating structure for CLIC led to two main results. The first is a strongly tapered structure design to restart the high-power testing program after the CLIC base frequency was changed from 30 GHz to 12 GHz in 2007. The second is a refined design of such structure with reduced tapering and improved rf-to-beam efficiency. Both structures have been produced first without and then with damping waveguides for damping of wakefields.

After this digression on the microscopic dynamics of vacuum discharges, our focus shifts to what are the macroscopic effects of rf breakdowns in accelerator structures. To begin with, in the next chapter we discuss rf-based measurements of breakdown during the high-gradient test of a CLIC prototype structure.

5. Diagnostics of rf breakdown

The study and understanding of the breakdown mechanism has historically been based on "macroscopic" observations, e.g. measurements of voltages, fields and currents arising during a breakdown. Only recently the microscopic observation of the breakdown site in an electron microscope set-up, where breakdown can be induced and observed, has become possible [47]. That is, however, limited to the use of static electric fields. Numerical simulations support and integrate such observations also in the case of rf fields but computational limits in terms of time and resources are still an issue.

With the only exception of the Two-beam Test Stand, where the performance of high-gradient accelerator structures can be investigated in the presence of an electron beam actually accelerated in the structure under study, high-gradient structures are usually not tested in real accelerator but rather in dedicated rf test stands. There, they are fed with rf produced by conventional sources and power levels and in some cases also currents, light and vacuum levels are measured. This is, for instance, the case at the Accelerator Structure Test Stand at SLAC where an extensive program of high-gradient accelerator structure testing was carried out for over a decade until 2012. It is with the high power test of an X-band CLIC prototype accelerator structure conducted there, and with the analysis of the data collected during such test, that this chapter is concerned. That is also the subject of Paper II, which is only briefly summarised in what follows, and is completed here with a detailed explanation of the analysis methodology.

5.1 Test of a structure assembled in a resonant ring

The diagnostics of rf breakdown discussed hereafter is based on the data collected from the high-gradient test of a travelling wave accelerator structure assembled in a two-arm resonant ring, which is a waveguide loop meant to build up power by constructive interference of a circulating rf field. A sketch of the set-up is shown in Fig. 5.1. A 50 MW klystron, on the right of Fig. 5.1, produces the rf power which is equally split to simultaneously feed the two arms of the ring through hybrid couplers. Each arm is equipped with directional couplers installed at the

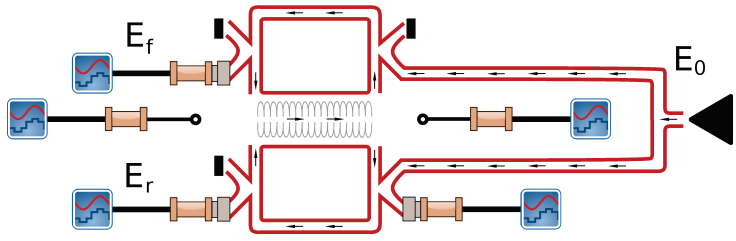

Figure 5.1: Travelling wave accelerator structure under test in a dual-arm resonant ring. the rf produced by a conventional source on the right of the Figure, is equally split to simultaneously feed the two arms of the ring through hybrid couplers. Each arm is equipped with directional couplers installed at the input and output ports of the structure for rf measurements. Additionally, two current detectors are installed at the two ends of the structure, facing the aperture, for dark current and breakdown current measurements.

input and output ports of the structure for rf measurements. Additionally, two current detectors are installed at the two ends of the structure, facing the aperture, for dark current and breakdown current measurements.

The rf picked up by the directional couplers is mixed with a local oscillator and shifted to an intermediate frequency of about 222 MHz, and it is finally sampled at a frequency of 2 GHz. The fast oscillating field at the sum frequency is discarded with an analog low-pass filter before the digitisation. Further treatment of rf signals is carried out off-line, as described in the next section.

5.2 Estimation of breakdown location

Most of the numerical treatment of rf signals discussed hereafter, was developed to estimate the location of breakdowns in the structure under test from measurements of rf power and phase. For this purpose, it is convenient to use a complex representation of the measured signals.

Any real signal can be written as

$$x(t) = A(t)\sin\left(\omega t + \phi(t)\right) \tag{5.1}$$

which can be represented with a complex signal $x_a(t)$ whose real part $x(t)$ is the original real signal and whose imaginary part $\hat{x}(t)$ is the same real signal shifted by a quarter cycle or $\frac{\pi}{2}$. Such complex signal is called analytic signal and is

$$x_a(t) = x(t) + i\hat{x}(t) \tag{5.2}$$

A real signal can be shifted by a quarter cycle by means of the Hilbert transform [48, see chap. 6], which has the advantage of shifting all the

frequency components by the same mount. If we call $\mathcal{H}$ the Hilbert transform operator, the analytic signal in Eq. 5.2 can be written

$$\begin{aligned} x_a(t) &= x(t) + i\mathcal{H}\left[x(t)\right] \\ &= A(t)\left[\sin\left(\omega t + \phi(t)\right) + i\sin\left(\omega t + \phi(t) + \frac{\pi}{2}\right)\right] \\ &= A(t)\left[\sin\left(\omega t + \phi(t)\right) + i\cos\left(\omega t + \phi(t)\right)\right] \\ &= A(t)i\left[\cos\left(\omega t + \phi(t)\right) - i\sin\left(\omega t + \phi(t)\right)\right] \\ &= A(t)e^{-i(\omega t+\phi)} \end{aligned} \tag{5.3}$$

In this representation, the amplitude and the phase of the real signal are given by the modulus and the argument of the analytic signal, respectively, as follows:

$$A(t) = |x_a(t)| \tag{5.4}$$

$$\omega t + \phi = \arg\left[x_a(t)\right] \tag{5.5}$$

When the rf is reflected during a breakdown it arrives at the input coupler with a phase different from that of the recirculating, or forward, field measured at the same coupler. That difference "contains" the memory of the breakdown location, given that the phase advance per cell in the structure is known. This way the location of the breakdown can theoretically be estimated with the resolution of one cell. Nevertheless, such estimation is not unique because of the ambiguity given by the fact that the phase is periodic every three cells, for this particular design. That can be fixed by adding to the picture the information on the arrival time of the reflected signal, whose delay after the reflection is of the order of several nanosecond because of the low group velocity in the structure, and it is therefore measurable.

The phase difference between forward and reflected signals is based on their complex representations

$$E_f(t) = E_f \exp\left[i\left(\omega t + \psi_f\right)\right] \tag{5.6}$$

$$E_r(t) = E_r \exp\left[i\left(\omega t + \psi_r\right)\right] \tag{5.7}$$

Both the forward field $E_f(t)$ and the reflected field $E_r(t)$ are numerically mixed with an oscillating signal of angular frequency $\omega + \Delta\omega$ ($\Delta\omega \ll \omega$) and phase θ to obtain the slow-varying signals

$$\tilde{E_f}(t) = E_f e^{-i[\Delta\omega t - (\psi_f - \theta)]} \tag{5.8}$$

$$\tilde{E_r}(t) = E_r e^{-i[\Delta\omega t - (\psi_r - \theta)]} \tag{5.9}$$

where the fast oscillating mixing product at the sum frequency is removed by passing the mixing product through a single pole infinite impulse response filter with a cut-off frequency of 500 MHz. The instantaneous phases of the slow signals are

$$\chi(t) = \arg\left[\tilde{E}_f(t)\right] = \Delta\omega t - (\psi_f - \theta) \tag{5.10}$$

$$\xi(t) = \arg\left[\tilde{E}_r(t)\right] = \Delta\omega t - (\psi_r - \theta) \tag{5.11}$$

Hence the phase difference δ between forward and reflected field is

$$\delta = \chi(t) - \xi(t) = \psi_f - \psi_r \tag{5.12}$$

Such phase difference calculated for a set of 107 breakdowns is shown in Fig. 5.2, where the three distinct populations which are about 120° apart suggest that the rf reflection plane is uniquely localised in one cell of the $\frac{2\pi}{3}$ structure. Moreover, because the electric fields assume their extreme values on the irises of each cell, there is higher the probability that a breakdown is triggered.

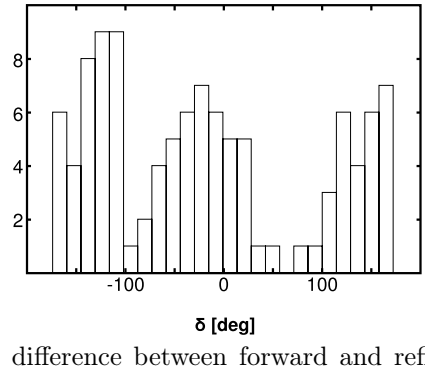

Figure 5.2: Phase difference between forward and reflected field in breakdowns. The three distinct populations separated by about 120° suggest that the rf reflection plane is uniquely localised in one cell of the $\frac{2\pi}{3}$ structure.

As anticipated, the phase information is not sufficient to localise uniquely the breakdown location, or more precisely the rf reflection plane, because of the periodicity of the result. That can be solved on the basis of the analysis of the power measurements. The filling time of the 18-cell structure is, in fact, 38 ns, which corresponds roughly to a filling time of 2 ns per cell. That causes a measurable delay between the power signals, which we use to estimate the breakdown location. To explain how, we refer to an example of rf signals measured in a breakdown event and shown in Fig. 5.3. There, it can be noted that the forward signal, i.e. the recirculating field, drops after the fast rise of the reflected signal. The time at which that happens is, however, simultaneous to the rise of the

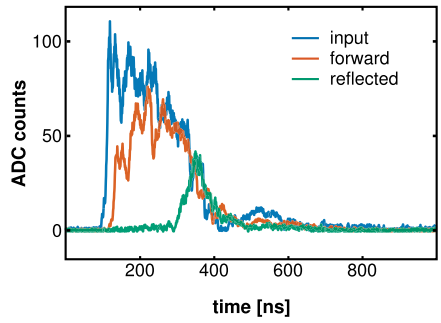

Figure 5.3: Example of rf signals measured during a breakdown. The input power (blue signal) is measured before being equally split into the two arms of the resonant ring. The recirculating field (orange signal) and the reflected field (green signal) are measured in one of the two arms. When a breakdown occurs after about 470 ns part of the power is reflected towards the input port of the structure and the forward signal, i.e. the recirculating field, drops to zero.

reflected signal, and the delay is due to the travel time of the field in the ring. Given the group velocity of the field in the ring, is therefore possible to reconstruct the location of the breakdown from the comparison of rising and falling edges of the power measurements. That is explained in detailed in Paper II. Here we only point out that the application of this methodology to the complete data set of breakdown events, resulted in the distribution of the number of breakdowns per cell shown in Fig. 5.4. There, it can be noted that the increasing number of breakdowns towards the output port of the accelerator structure is compatible with its tapered design.

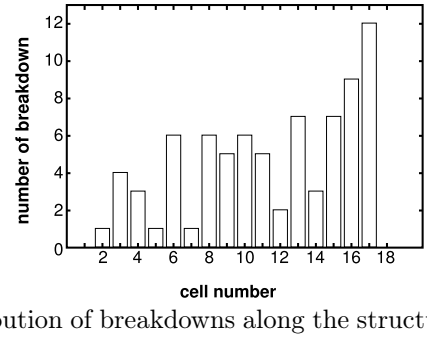

Figure 5.4: Distribution of breakdowns along the structure is peaked towards the structure output port, in agreement with the tapered design of the structure.

The complex representation of the field is also handy because phase shift and attenuation in the resonant ring can be conveniently represented by the real and imaginary part of a complex number, respectively. In this way the recirculation of the rf can be described at any time in

terms of a linear combination of input and forward fields and in terms of complex parameters that express the attenuation and phase advance in the loop. Because the rf pulse is about 200 ns long and it is sampled with a frequency of 2 GHz, we have a linear system of about 400 equations which can be solved in the least square sense in order to estimate the complex parameters that describe attenuation and phase advance in the ring. Such least square procedure is discussed, for instance, in Ref. [49, chap. 15.4] for real data and it is applied in this context to a set of complex data as discussed in Paper II.

5.3 Estimation of breakdown plasma density

The same complex representation used for the estimation of the characteristics of the resonant ring in case of no breakdown is used to describe the field recirculation when a breakdown occurs. That takes into account the reflected field and the power absorbed in the breakdown process or missing energy. The field reflection from a breakdown can be thought of as the reflection in case of the presence of a mismatched load in the structure, with the peculiarity that the load is represented in this context by the plasma that builds up during the discharge.

With that in mind we assumed a simple plasma model, quasi-neutral, non-collisional and magnetised, for which the permittivity has a simple analytical form which depends on the electron density. The reflection coefficient associated to such permittivity can also be calculated and thence the electron density estimated for any breakdown event, which we find to be about 10^{16} electrons per cubic centimetre.

For a more complete derivation of this result, the reader should refer to Paper II.

So far, we have discussed rf measurements of breakdowns in a CLIC prototype accelerator structure. In the next chapter, we shifts our focus on the impact that breakdowns have on the accelerated beam, on the basis of experimental observations carried out at the CTF3 Two-beam Test Stand.

6. Effects of rf breakdown on the beam

The study of the effects that rf breakdowns have on the beam is an important aspect in the development of future high energy linear colliders as CLIC, because of the impact that such effects can have on the collider luminosity. Simulations and measurements of rf breakdowns in X-band accelerator structures have shown that both the transverse and the longitudinal beam momentum can be affected [50]. Moreover, it has been suggested that in high-gradient accelerator structures simply dark currents can kick the beam in the transverse plane even if no breakdown occurs [51]. In the past, an attempt to measure such effects was made at SLAC where transfer of transverse momentum to the beam in case of rf breakdowns, so-called breakdown kick, was observed and its magnitude experimentally measured and found to be of the order of 10 to 30 keV/c [50, 52].

The continuation of the studies of effects of rf breakdowns in CLIC structures was identified as one of the main scientific goals of the CTF3 Two-beam Test Stand. For this purpose, the Two-beam Test Stand is equipped with diagnostics to measure beam position, beam energy and beam profile before and after the acceleration section. Transverse kicks to the beam trajectory can be detected through beam position measurements or through measurements of the beam profile. Energy variations can be determined by measuring the beam position or the beam profile in the spectrometer line.

6.1 Beam trajectory

The expected angular deviation to the 180 MeV probe beam for transverse kicks of 10 to 30 keV/c is 56 to 160 µrad. On the basis of these expectations, the probe beam line in TBTS is equipped with five BPMs installed before and after the accelerator structure, in order to detect transverse kicks to the beam trajectory, as described in Ref. [53]. A resolution of 10 µm on the measurement of the beam position along a single bunch-train is required to resolve transverse kick angles of 10 µrad. The same resolution allows to resolve beam energy variation in the spectrometer line of the order of 10^{-5}.

As a preliminary step, the calibration and resolution of the BPMs were thoroughly investigated, and are documented in Paper V. The resolution

of one BPM is defined as the standard deviation of the distribution of the residuals given by comparing the beam position measured at that BPM with the beam position expected at the same BPM and estimated through the measurements of any other two BPMs in the beam line. An example of beam current and position measured with one of the BPMs is shown in Fig. 6.1. It is worth stressing that in this context we are not

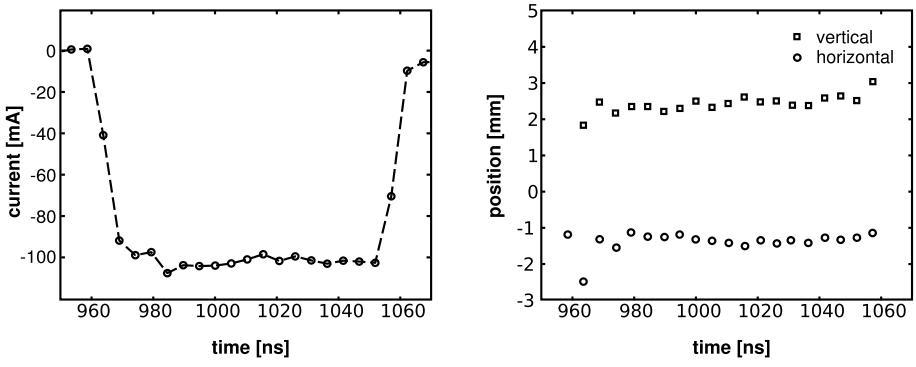

(a) **(b)**

Figure 6.1: Example of measurement of (a) beam current and (b) beam position with an inductive Beam Position Monitor in the probe beam line of the Two-beam Test Stand.

interested in the average position of the bunch-train at one BPM which is currently referred to as beam orbit, but rather in the time-resolved measurement of the position of a bunch-train at one BPM. An example of the result of the resolution measurement is shown in Fig. 6.2, where on the right we show the distribution of the residuals obtained averaging the beam position measurement in Fig. 6.1b over the whole bunch-train, whereas on the left we show the distribution of the residuals obtained from the same measurements of beam position time-resolved along the bunch-train. In the former case, the resolution is 20 µm whereas in the latter case it is limited to 110 µm. The reason for that has to do with the design of the BPMs, which was optimised for the multi-ampere drive beam [37]. In the probe beam line, where the beam current is about hundred times lower, it was not possible to achieve the desired spatial resolution, due to the much smaller signal-to-noise ratio.

In 2012 two cavity BPMs were installed in TBTS. They were originally designed as prototype monitors for TeV colliders within the EUROTeV project [54]. They have subsequently been optimised for the CALIFES linac and finally installed in the TBTS to provide better resolution with respect to the inductive BPMs. Unfortunately, only two such BPMs were available and it was decided to install them after the acceleration section,

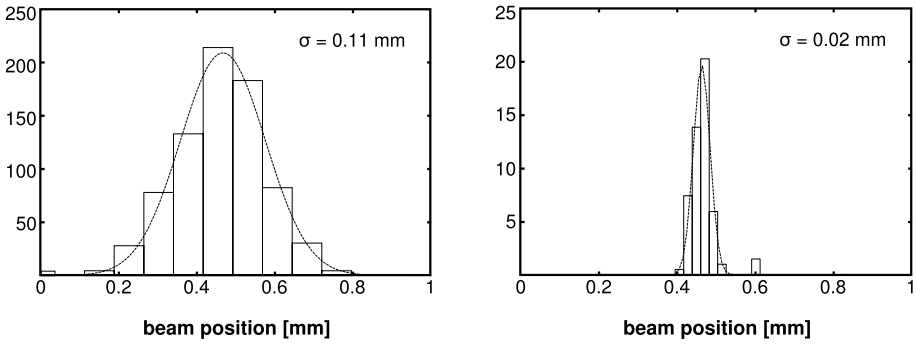

(a) resolution along single bunch-trains

(b) resolution of average bunch-train position

Figure 6.2: Example of distribution of residuals between expected and calculated position of the beam at one BPM in the probe beam line of the Two-beam Test Stand. The wider distribution on the left (a) is based on the position of the beam along single bunch-trains whereas the narrower distribution (b) is based on beam positions averaged over the whole bunch-train.

before the imaging screen. In such configuration, it was only possible to detect variation of the beam trajectory along the same bunch-train.

6.2 Beam profile

The first successful attempt to measure the effects on the beam of rf breakdowns in the CLIC prototype accelerator structure installed in the Two-beam Test Stand, was based on measurements of the transverse beam profile on a scintillating screen before the spectrometer line, about 4.8 m downstream of the accelerator structure. That screen was chosen instead of the one in the spectrometer line because the beam trajectory could be made ballistic up to that point by turning the quadrupoles off, in order to facilitate the interpretation of the measurements.

Double beam spots were occasionally observed in case of breakdowns, which we explained as resulting from a change of the beam trajectory during the pulse: part of the pulse is kicked in the transverse plane, travels on a different orbit and hits the screen at a different point. An example of beam profile is shown in Fig. 3.6a, where the double spot is caused by a transverse kick to the beam in the vertical plane. Similar beam profiles caused by transverse kicks in the horizontal plane where also measured. From the measurement of the beam profile, the angular magnitude of the transverse kick to the beam can be easily estimated. Because the beam trajectory was ballistic between the accelerator structure and the screen, given the distance d between the centroids of the two measured spots, the kick angle is $\theta \simeq d/L$, where L is the distance

between the accelerator structure, for instance its centre, and the screen. The distance d was calculated by fitting the sum of two two-dimensional Gaussian functions to the data. The assumption that the beam is kicked at the centre of the 23 cm long accelerator structure is arbitrary, but it does not affect the order of magnitude of the estimated kick angle. Nevertheless, it introduces a systematic error of about 0.024 mrad. That can be reduced by about ten times, by taking into account the breakdown location estimated from the rf measurements, as discussed in the previous chapter.

Finally, it is worth mentioning that to verify that additional spots on the beam profile were not caused by breakdown current hitting the screen, the measurement was repeated without the beam and that always led to a less bright, wider, and blurred image as shown in Fig. 6.3b.

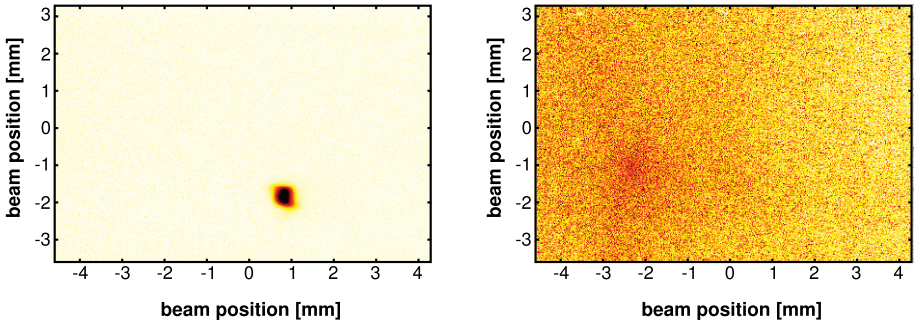

(a) **(b)**

Figure 6.3: (a) An example of beam profile measured during normal operation. (b) An image of breakdown current, i.e. electron current ejected from the accelerator structure during a breakdown when no beam is present. In this image, the gain is increased with respect to the image on the left.

6.3 Beam energy

From the measurements of beam profiles and trajectories after the acceleration section in the Two-beam Test Stand, two main effects have been identified which are related to the energy gained by the accelerated beam. The first effect has nothing to do with rf breakdowns and we refer to it as *acceleration kick*. It concerns misalignment between the beam trajectory and the axis of the accelerator structure. A second effect that we call *lack of acceleration*, concerns the case in which due to an rf breakdown the beam gets accelerated less than nominally.

6.3.1 Acceleration kicks

In case of a misalignment between the beam trajectory and the axis of the accelerator structure, the beam is accelerated also transversely, which translates into a transverse displacement of the beam trajectory downstream of the accelerator structure. We call this effect *acceleration kick*. This effect was observed comparing the accelerated and the non-accelerated beam trajectories measured with one cavity BPM, an example of which is shown in Fig. 6.4, where the two trajectories are shifted by 0.26 mm. It is worth noting that the overshoot visible at the beginning of the signal is due to the readout electronics and that it is not related to the beam position.

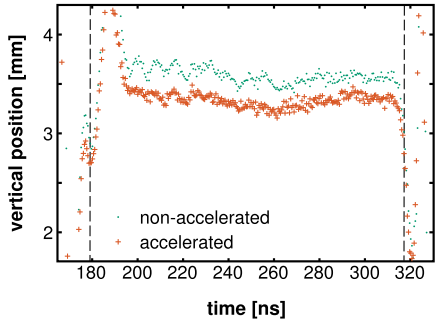

Figure 6.4: Example of beam trajectories measured at one BPM downstream of the accelerator structure, in case the beam is accelerated or not. The difference between the two measurements, which we call *acceleration kick*, is explained in terms of a misalignment between the beam orbit and the axis of the accelerator structure.

A typical probe beam bunch-train consists of 150 relativistic bunches. The time of flight of each one of them in the accelerator structure is about 0.8 ns, whereas the time of flight of the whole bunch-train is about 120 ns. Because the filling time of the 24-cell structure is 65 ns, almost 3 ns per cell, we assume that the available power does not change while a bunch travels through the structure, but variations are not negligible between two subsequent bunches. In other words, we assume that each bunch sees a static field $\mathcal{E}$ which is given by the square root of the power $P(t)$ in the structure at the time t at which the bunch enters it. The total energy gained by each bunch is therefore

$$E(t) = \sum_{j=0}^{N_{cell}} \mathcal{E}_j(t) = \sum_{j=0}^{N_{cell}} [P(t)_j]^{1/2} \tag{6.1}$$

If we neglect the beam loading in the accelerator structure, which is small for the probe beam, and in case no breakdown occurs, the whole bunch-train is accelerated with a constant gradient, as depicted in Fig. 6.5a.

If the beam trajectory has an angle with respect to the axis of the accelerator structure, part of the energy available accelerates the beam on the transverse plane. In that case, Eq. 6.1 can be rewritten in its longitudinal and transverse components, as follows:

$$E_{\parallel}(t) = \sum_{j=0}^{N_{cell}} \mathcal{E}_j(t)\cos(\theta) = E(t)\cos(\theta) \tag{6.2}$$

$$E_{\perp}(t) = \sum_{j=0}^{N_{cell}} \mathcal{E}_j(t)\cos(\theta) = E(t)\sin(\theta) \tag{6.3}$$

The angle θ can be estimated from the measurement of the displacement d of the trajectory of the accelerated beam with respect to the trajectory of the non-accelerated one. Similarly to the case of a breakdown kick, the misalignment angle is $\theta \simeq d/L$, where L is the distance between the BPM and the centre of the accelerator structure. We found that such angle is 0.57 mrad, which is consistent with the mechanical accuracy of the alignment of the structure in the beam line. It is worth noting that even if the beam could be steered to an orbit that was stable irrespective of whether the beam was accelerated or not, we chose to maintain the shift between accelerated and non-accelerated positions. That permits an indirect measurement of beam energy variations along a single bunch-train.

6.3.2 Effect of rf breakdowns on the beam energy

As discussed in Chapter 5, when a breakdown occurs the accelerator structure is effectively "shorted" and the power fed to it is partially reflected backwards, partially transmitted to the structure output port and partially dissipated in the discharge process. As a consequence, the energy available to accelerate the beam is less than the nominal, i.e. the beam is accelerated in a gradient lower than 100 MeV/m.

Here we discuss our understanding of such effect on the basis of experimental observations. In our analysis, we assume that the reflected field does not interfere with the forward field and we neglect the attenuation of the rf due to ohmic losses along the structure.

In case of a breakdown, Eq. 6.2 and Eq. 6.3 are still valid, but the field in the structure changes and the acceleration kick differs from bunch to bunch. In order to explain that, we first consider the case in which the forward power is completely reflected from the breakdown. We assume that the structure is already filled, i.e. provides the nominal accelerating gradient, and that a breakdown occurs at the longitudinal coordinate z_{BD}. From that moment on, nothing changes upstream of the breakdown

where the accelerating gradient remains constant as long as the structure is fed, whereas downstream of the breakdown the structure empties at a rate given by the group velocity of the field in the structure.

In such case Eq. 6.1 still holds and the field $\mathcal{E}_j(t)$ is a piecewise function defined as

$$\mathcal{E}_j(t) = \begin{cases} \max \mathcal{E}_j(t) & \text{when } z < z_{BD} \\ \max \mathcal{E}_j(t) & \text{when } z > z_{BD} + d_1 \\ 0 & \text{when } z_{BD} < z < z_{BD} + d_1 \end{cases} \tag{6.4}$$

where d_1 is the distance travelled by the field in the structure from the coordinate z_{BD} in the time t, being the time $t = 0$ set at the moment at which the breakdown occurs. Any bunch entering the structure after the breakdown will therefore not get the maximum acceleration and so will any subsequent bunches which will be less and less accelerated.

A few illustrative examples are sketched in Fig. 6.5. The case in which a breakdown occurs in the last cell of the structure is sketched in Fig. 6.5b and it is the only case in which the beam energy is not affected because each bunch sees a completely filled structure.

A completely opposite case is the one in which a breakdown occurs in the first cell of the structure, sketched in Fig. 6.5c. All the bunches entering the structure after the breakdown has occurred will see the structure only partially filled and will gain less and less energy until the structure is completely empty. Eventually, the tail of the bunch-train will not be accelerated at all. This scenario can be compared to the measurement of the beam trajectory in Fig. 6.6a. The position of the first part of the bunch-train - from 180 ns to 250 ns - is the same as the position of an accelerated bunch-train when no breakdown happens in the accelerator structure, i.e. the beam is fully accelerated. Afterwards the position shifts in about 10 ns vertically downwards by about 0.75 mm. It oscillates for the remaining length of the bunch-train but it never shifts back to its initial position. If we disregard the first 20 ns of such signals, we can identify two main trajectories: the first one corresponding to the fully accelerated beam and the second one corresponding to the beam affected by the breakdown.

Finally, the case in which a breakdown occurs in the middle of the structure is sketched in Fig. 6.5d. In that case the whole bunch-train will be accelerated by a minimum which corresponds to half of the maximum acceleration because only the second half of the structure empties.

So far we have implicitly assumed that the breakdown and therefore the reflection of power goes on indefinitely or longer than the time of flight of the whole bunch-train in the structure. We now consider that a breakdown has a finite duration Δt. Once it has ended, the power starts flowing again in the structure through the breakdown location z_{BD}. At

(a) In case of no breakdown, every bunch in the bunch-train is fully accelerated.

(b) If a breakdown occurs at the end of the structure we observe that rf is reflected backwards but the whole structure still provides full acceleration to each bunch.

(c) If a breakdown occurs at the beginning of the structure the whole structure starts emptying because most of the power is reflected backwards. The bunches entering the structure after the breakdown are not fully accelerated.

(d) If a breakdown occurs in the middle of the structure part of it starts emptying because most of the power is reflected backwards. The bunches entering the structure after the breakdown are not fully accelerated. If the breakdown lasts less than the time of flight in the structure of the remainder of the bunch-train, the structure starts filling again and from that moment onward the bunches gain more and more energy.

Figure 6.5: Sketches of how a bunch-train is accelerated in case of (a) no breakdown, in case a breakdown occurs at (b) the end or (c) the beginning of the structure, and (d) in case a breakdown occurs in any intermediate cell of the structure and lasts for a limited amount of time. The sketches on the left refer to what happens before the breakdown, whereas the sketches on the right refer to what happens after the occurrence of a breakdown.

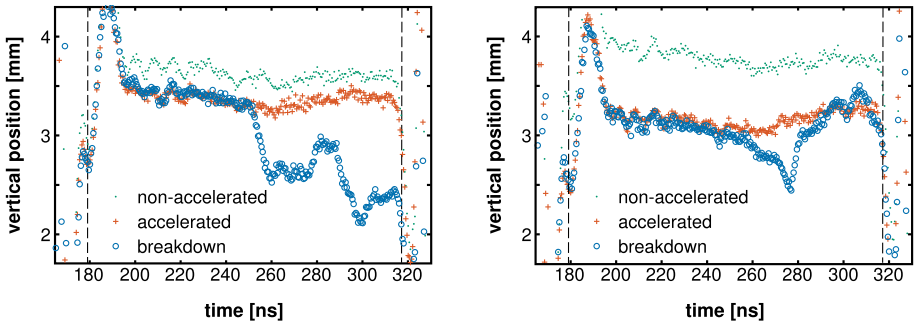

Figure 6.6: Example of vertical beam trajectories measured at one BPM downstream of the accelerator structure.

any time $t > \Delta t$ the field in the structure is

$$\mathcal{E}_j(t) = \begin{cases} \max \mathcal{E}_j(t) & \text{when } z < z_{BD} + d_2 \\ \max \mathcal{E}_j(t) & \text{when } z > z_{BD} + d_1 \\ 0 & \text{when } z_{BD} + d_2 < z < z_{BD} + d_1 \end{cases} \tag{6.5}$$

where d_2 is the distance travelled by the field in the structure from the coordinate z_{BD} in the time $t - \Delta t$. This scenario can be compared to the measurements in Fig. 6.6b, where the beam trajectory has a dip in correspondence of a breakdown which lasts for about 20 ns. In this case, during the breakdown the beam is pushed away from the trajectory of the non-accelerated beam, suggesting that little or no contribution comes from lack of accelerating gradient after the breakdown location or that the breakdown happened towards the output port of the accelerator structure. The estimation of the breakdown location based on rf measurements for this event supports indeed the latter hypothesis, i.e. that the breakdown happened in the last cell of the accelerator structure.

To test the explanation that we offered to describe a breakdown in the accelerator structure and its effect on the beam trajectory and energy, we try to predict how the beam profile in presence of a breakdown looks on the imaging screen. According to what discussed above, we expect it to be a mixture of both the non-accelerated and the accelerated beam profiles. The contribution of each one of them is calculated along the bunch-train, according to how close the beam trajectory corresponding to the breakdown is to the accelerated or the non-accelerated ones. The result obtained is shown in Fig. 6.7a for one breakdown event and can be compared with the real measurement shown in Fig. 6.7b.

We want to stress that the displacement of the beam position in case of an rf breakdown can be due to two different effects, the lack of power in

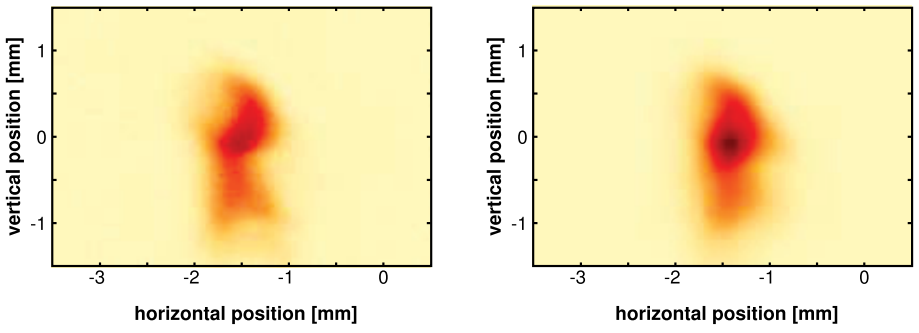

(a) **(b)**

Figure 6.7: Predicted (left) and measured (right) breakdown beam spot.

the structure due to its reflection and the direct effect of the breakdown on the beam. When both affect the beam position in the same direction the two effects cannot be disentangled, unless the beam energy is also measured. That was not possible in our experiment because the beam position monitor in the spectrometer line was obscured by the screen used in our measurements.

6.3.3 Beam profile shape and orientation

An example of acceleration kick is shown by the measurement of the beam profile in Fig. 6.8a. There, it can be observed that the beam centroid is displaced vertically downward when the beam is accelerated. Moreover, it can also be observed that its shape and orientation are different from the ones of the non-accelerated beam profile shown in Fig. 6.8b. The beam profile corresponding to the non-accelerated bunch-train is elliptical and tilted, which indicates coupling between the horizontal and the vertical plane. This coupling is caused by the solenoids surrounding the CALIFES accelerator structures to provide transverse focusing when the beam is generated and accelerated before being sent to the Two-beam Test Stand. Since no solenoidal field or skew quadrupole is present in the Two-beam Test Stand, we attribute the change in size and orientation of the accelerated bunch-train profile to the field in the accelerator structure. If we consider that the beam size is almost doubled with respect to the non-accelerated one, such change can be accounted for by a defocusing quadrupole with a focal length of about 5 m. This effect can be explained if we consider that a quadrupolar component of the fundamental accelerating mode is present in both the input and output couplers of the accelerator structure due to the symmetry broken by the presence of two feeding waveguides. Moreover, the presence of wakefield-damping waveguides which breaks the symmetry of all regular cells in the struc-

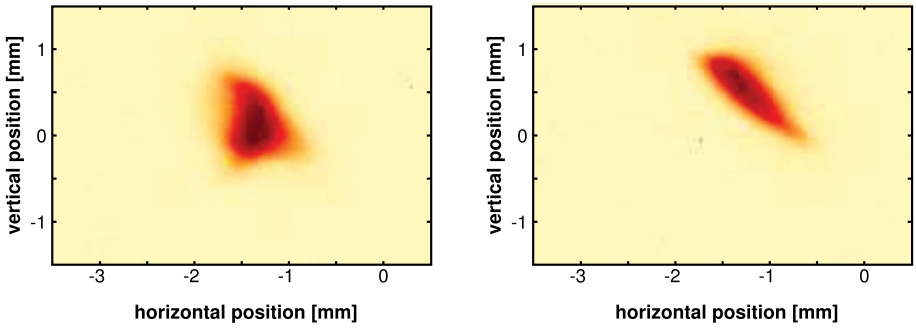

Figure 6.8: Images of the beam profile when the beam is accelerated (left) and when it is not accelerated (right).

ture, introduces an octupolar component of the fundamental mode. The integrated strength of such additional multipolar modes were calculated for a CLIC baseline accelerator structure [55] and resulted in 17×10^{-3} T integrated throughout the input and output couplers and 8×10^{5} T m^{-2} integrated throughout all regular cells of the accelerator structure. For a beam energy of 180 MeV the quadrupolar field component contributes with a focal length of about 30 m, which is not enough to explain our observation. On the other hand, the slope of octupolar field component in the regular cells at a beam offset of 200 µm in the structure produces a quadrupolar effect with a focal length of about 5 m. Thus, the effect of the octupolar mode in the regular cells of the accelerator structure can account for the observed focusing effect.

6.4 Statistics

The analysis described was applied to a data set of 246 breakdowns collected during about 12 hours.operation during the summer 2012, dedicated to the optimisation and stabilisation of the experimental conditions. The histogram in Fig. 6.9 shows the distribution of the total angular magnitude of transverse kicks to the beam, whose average magnitude is 0.16 ± 0.08 mrad or 29 ± 14 keV/c. As discussed, this estimation is biased by the effect of the transverse beam acceleration due to the misalignment of the accelerator structure and the beam trajectory. Nevertheless, from the analysis of only the non-breakdown events we deduce that the maximum magnitude of such acceleration kick is about one third of the average magnitude of the kick distribution presented in Fig. 6.9. In other words, the distribution in Fig. 6.9 represents mainly the effect of breakdown kicks, because the contribution of acceleration kicks is smaller than 30%.

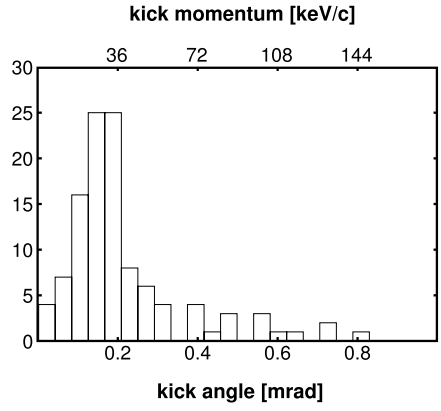

Figure 6.9: Distribution of the magnitude of breakdown kicks to the beam trajectory.

Finally, we found that there is no correlation between the kick angle and the location of the breakdown in the accelerator structure, as shown in Fig. 6.10a. Moreover, as shown in Fig. 6.10b, we found that there is also no correlation between the kick angle and the energy dissipated in the breakdown, which is calculated as the difference between the energy fed to the structure and the energy transmitted to the structure output plus the energy reflected to the structure input, taking into account the attenuation due due to ohmic losses.

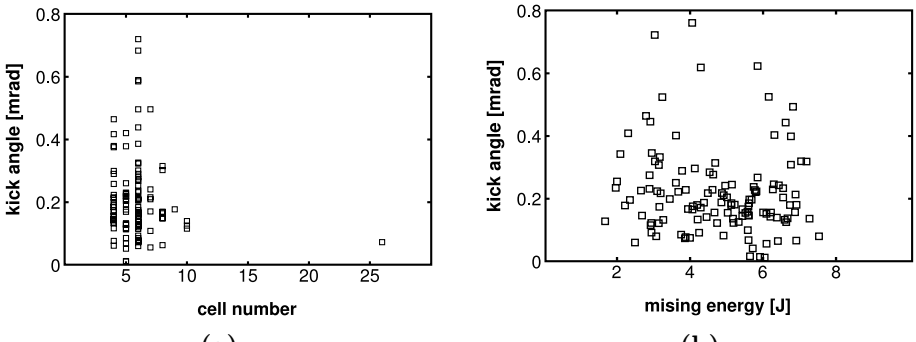

Figure 6.10: Correlation between kick angles and (a) the breakdown location in the accelerator structure, or (b) the energy dissipated in the breakdown.

In this chapter, we have shown and discussed measurements of the effects of rf breakdowns on the beam in the CLIC prototype accelerator structure tested at the Two-beam Test Stand. In the next chapter, we discuss the impact of our findings on the CLIC main beam and discuss the implications that they have on the CLIC performance.

7. Effects of rf breakdown on CLIC luminosity

In the previous chapter we discussed the effects of an rf breakdown in a CLIC prototype accelerator structure on the beam. First, we found that transverse momentum can be transferred to the beam. Second, we found that the beam energy can also be affected. Finally, we observed a focusing effect on the beam in case of beam-structure misalignment. We expect that each one of these effects will cause beam filamentation and consequent emittance growth, which translate, if applied to the CLIC main beam, to a degradation of luminosity.

Geometric luminosity loss in case of full beam filamentation has been calculated in the case of transverse kicks, betratron mismatches, beam energy loss and mismatches due to skew quadrupolar errors, which are thoroughly discussed in Paper VI. Here we summarise the results in case the effects of rf breakdown measured at the TBTS are assumed and applied to the CLIC main beam.

7.1 Transverse kicks

We found that the magnitude of transverse momentum transferred to the beam when an rf breakdown occurs in an accelerator structure has an average value of 29 keV/c. That translates to an angular kick of about 0.16 mrad for the 180 MeV probe beam as measured at the TBTS. The same transverse momentum transferred to the CLIC main beam at the injection energy of 9 GeV translates to an angular kick of 3 µrad and to only 19 nrad in case it occurs at the main beam maximum energy of 1.5 TeV. A summary of the principal nominal beam parameters at the beginning and at the end of the main linac is given in Tab. 7.1. It is worth comparing the magnitude of the angular kicks with the natural beam divergence. We note that the beam divergence σ' scales with the inverse root of the Lorentz factor γ:

$$\sigma' = \sqrt{\frac{\epsilon_n/\gamma}{\bar{\beta}}} \tag{7.1}$$

where we considered the ultra-relativistic case, $\bar{\beta}$ is the Twiss parameter of the beam and ϵ_n is the normalised beam emittance. On the other hand, the kick angle θ for a transverse momentum of 29 keV/c scales

Table 7.1: CLIC main beam parameters.

beginning of main linac	
energy	9 GeV
horizontal emittance (norm.)	600 nm rad
horizontal emittance	34 pm rad
horizontal beam divergence	1.80 µrad
vertical emittance (norm.)	10 nm rad
vertical emittance	0.6 pm rad
vertical beam divergence	0.24 µrad
end of main linac	
energy	1.5 TeV
horizontal emittance (norm.)	660 nm rad
horizontal emittance	0.2 pm rad
horizontal beam divergence	0.14 µrad
vertical emittance (norm.)	20 nm rad
vertical emittance	7 fm rad
vertical beam divergence	26 nrad

with the inverse of γ, therefore the angular kick magnitude in terms of beam divergence scales with the inverse square root of γ. At the beginning of the linac, the ratio θ/σ' between a breakdown kick and the beam divergence is 1.8 in the horizontal plane and 13 in the vertical plane. At the end of the linac, on the other hand, the same ratio is 0.14 in the horizontal plane and 0.73 in the vertical plane.

In order to calculate what is the effect of a kick on the luminosity, we assume that the beam is Gaussian and that all particles receive a transverse kick of magnitude θ. All of them will then start betatron oscillations at different angles and during their passage down the linac they will span all the phases. That can be conveniently calculated in terms of action angle variables (J, ϕ) in the normalised phase space $(\tilde{x}, \tilde{x}')$, where the full beam filamentation is calculated by integrating the beam distribution $\Psi_f(J, \phi)$ over the angle variable ϕ. That gives [56]

$$\Psi_f(J) = \frac{1}{2\pi\epsilon}\left[-\frac{J}{\epsilon} - \frac{\beta\theta^2}{2\epsilon}\right] I_0\left(\frac{\sqrt{2J\beta}\theta}{\epsilon}\right) \tag{7.2}$$

where I_0 is the Bessel function of zeroth order. Fig. 7.1 shows the projection of the fully filamented distribution in Eq. 7.2 onto one dimension in normalised phase space, for a kick amplitude of 29 keV/c caused by

an rf breakdown at the main linac injection energy of 9 GeV and at the final energy of 1.5 TeV. There, we see that the beam distribution is basically unaffected at high energy whereas the effect of the breakdown kick is more severe at low energy, in which case it is worse in the vertical plane. We assume that the beam is uncoupled and that the kick affects

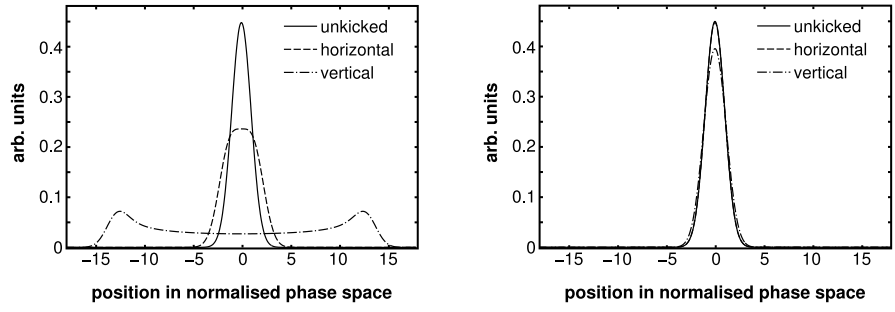

Figure 7.1: Projection of the fully filamented distribution onto the $\tilde{x}$-axis in normalised phase space, for different normalised kick amplitudes caused by an rf breakdown (a) at the main linac injection energy of 9 GeV and (b) at the final energy of 1.5 TeV.

the beam either in the horizontal or in the vertical plane. Moreover, we assume that no strong beam-beam effect is present and thus we calculate the luminosity loss as the overlap integral of two Gaussian distribution, one of which is the kicked distribution in Eq. 7.2. We found that the luminosity loss is small if the kick occurs at high energy, where it results in a few per mille in the horizontal plane and 2.4% in the vertical plane. It is instead more relevant if the kick occurs at low energy, where it is 30% in the horizontal plane and more 91% than in the vertical plane.

7.2 Betatron mismatch

The same reasoning applied to the case of a transverse kick can be applied to the case of a betatron mismatch. That is the case where the Twiss parameters of the beam are different from those of the lattice. In this case, the beam distribution after full filamentation is [57]

$$\Psi_f(J) = \frac{1}{2\pi\epsilon} e^{-B_{mag}J/\epsilon} I_0\left(\frac{J}{\epsilon}\sqrt{B_{mag}^2 - 1}\right) \tag{7.3}$$

where B_{mag} is the so-called emittance growth factor

$$B_{mag} = \frac{1}{2}\left[\left(\frac{\bar{\beta}}{\beta} + \frac{\beta}{\bar{\beta}}\right) + \beta\bar{\beta}\left(\frac{\bar{\alpha}}{\bar{\beta}} - \frac{\alpha}{\beta}\right)^2\right] \tag{7.4}$$

which quantifies the growth of the transverse beam emittance in terms of the Twiss parameters of the beam, α and β, and of the lattice, $\bar{\alpha}$ and $\bar{\beta}$.

A betatron mismatch can occur, for instance, in case of a quadrupolar error like the one observed during beam acceleration in case of a misalignment between the beam and the accelerator structure. In that case we found that the focusing effect observed can be accounted for by a quadrupolar field with a focal length of 5 m. We can therefore relate B_{mag} to an integrated quadrupolar field characterised by its focal length f, which gives

$$B_{mag} = 1 + \frac{\beta^2}{2f^2} \tag{7.5}$$

The beam distribution in Eq. 7.3 after full filamentation is shown in Fig. 7.2, where the emittance growth factor B_{mag} is calculated for $f = 5$ m in the case of the CLIC betatron length of 10 m, and compared to the unkicked beam distribution. In this case, the relative luminosity loss is about 30%.

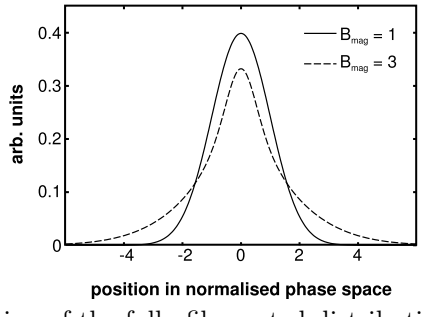

Figure 7.2: Projection of the fully filamented distribution onto the $\tilde{x}$-axis in normalised phase space, characterised by different values of B_{mag}.

7.3 Energy loss

In case of beam energy loss, the lattice which is initially matched to the beam, suddenly becomes too strongly focusing and the beam undergoes filamentation. This scenario is equivalent to that of a quadrupolar error in which case the beam suddenly passes through an unmatched lattice.

We observed that an rf breakdown causes lack of acceleration because a fraction of the power fed to the structure is reflected and thus not available to accelerate the beam. As discussed in the previous chapter, the worst case scenario corresponds to an energy deficit of about 23 MeV, which is the maximum energy gained in one accelerator structure operated at the nominal gradient of 100 MV/m. That corresponds

to a relative momentum loss $\delta = \frac{\Delta p}{p_0}$ of 2.5×10^{-3} at the main beam injection energy of 9 GeV or a relative momentum loss of 1.5×10^{-5} at the main beam maximum energy of 1.5 TeV.

The explicit dependence of B_{mag} on the relative momentum loss δ is shown in Fig. 7.3, where the emittance growth factor is plotted for different phase advance per cell among which the nominal value for the CLIC main linac of 72°. It can be noted that the increase of B_{mag} is larger in the defocusing plane, as shown in Fig. 7.3b, where it is anyway smaller than 4×10^{-6}. The loss in the geometric luminosity will therefore be negligible.

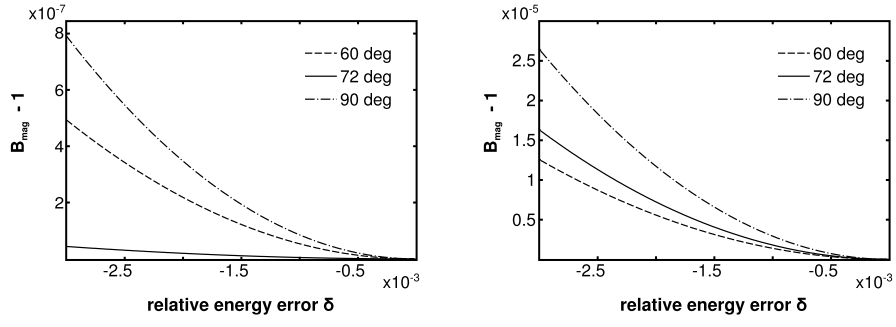

(a) **(b)**

Figure 7.3: The effective betatron mismatch parameter B_{mag} versus the relative momentum loss δ resulting from energy loss before either the focusing (left) or the defocusing (right) quadrupole. Here we compare the case FODO lattices with 30, 60 and 90° phase advance per cell with the nominal value for the CLIC main linac of 72°.

8. Conclusions

This study was set out to investigate the impact that vacuum discharges, or rf breakdowns, in high-gradient accelerator structures have on the beam. That is one of the key feasibility issues on the road map towards the realisation of a linear collider based on CLIC technology, because it can lead to a severe degradation of the collider luminosity. In this thesis we reported on experimental observations of such effects through rf-based and beam-based diagnostics, and we discussed their impact on the CLIC performance.

The test bed for our study was the Two-beam Test Stand, an experimental area built at the CLIC Test Facility 3 at CERN to test the feasibility of the CLIC technology. There, we demonstrated the feasibility of the CLIC two-beam acceleration technique even beyond the required accelerating gradient of 100 MeV/m. On the basis of previous experiments and simulations that identified transfer of transverse momentum to the beam as one of the effects of rf breakdowns, we based our search on measurements of beam trajectory, beam profile and beam energy. Moreover, we completed our observations with measurements of rf power in the CLIC prototype accelerator structure under test.

Experimental methods based on the analysis rf-based measurements were developed in the context of the high-power test of a CLIC prototype accelerator structure assembled in a resonant ring at the Accelerator Structure Test Stand at SLAC. There, we implemented a method to uniquely determine in which cell of the structure an rf breakdown occurs, on the basis of measurements of power and phase. Moreover, we applied a simple plasma model to describe the rf reflection observed during a breakdown and we estimated its density in about $10^{16}\,\mathrm{cm}^{-3}$.

The methods developed to identify breakdown locations in an accelerator structure, was then used to study the effects that rf breakdown have on the beam. We confirmed that in case of breakdowns transverse momentum can be transferred to the beam, and we found that its magnitude is 29 ± 16 keV/c. Moreover, we found that it is not correlated to where the breakdown occurs in the structure, nor to the energy absorbed during the breakdown process. That suggests that irrespective of the conditions at which the structure is operated, we can always expect that transverse momentum can be transferred to the beam within the measured limits, and that the beam trajectory is kicked by an angle which depends only on the longitudinal beam momentum. In the context

of the CLIC main linac, where the colliding beams need to be aligned with a nanometric accuracy, we expect that transverse kicks to the beam due to rf breakdowns will lead to beam emittance growth, with subsequent degradation of the collider luminosity. We found that transverse kicks can cause up to 90% of geometric luminosity loss if occurring at the injection energy of 9 GeV as opposed to a few per cent in case they occur at the final energy of 1.5 TeV.

In addition to transverse kicks to the beam trajectory, we observed that the longitudinal acceleration can also be affected by breakdowns. That is because an accelerator structure is effectively shorted during a breakdown, and a significant fraction of the power is reflected and not available to accelerate the beam. We found that this effect depends on where the breakdown occurs in the structure, and in the worst case scenario it leads to a complete lack of acceleration. This effect was also studied in the context of the CLIC main linac, and we found that it has a negligible effect on the luminosity, irrespective of the energy at which it occurs.

The analysis presented in this thesis is based on a poor statistics, which is mainly due to the difficulties arising from the instabilities of the CTF3 drive beam. With more stable beam conditions, it would be possible to extend our study to investigate the dependence of breakdown kicks on rf power level and pulse length. Moreover, beam energy variations need to be measured directly with a higher accuracy, which could be done with an additional high-resolution BPM in the TBTS spectrometer line. Finally, a bigger number of high-resolution BPMs also before the acceleration section, could be used to measure trajectory variations with a higher accuracy, because they could be decoupled from upstream beam instabilities.

Acknowledgements

It was almost five years ago when I first moved to Uppsala. Now that I am wrapping things up I can't help thinking how fast all these years have passed and how packed of experiences they have been. I risk to be lengthy here, but I want to take this opportunity to thank each and everyone who had a part in this course.

First of all, my gratitude goes to those who nourished my interest in the field of accelerator physics when I first came across it as an undergraduate student in Rome. I must give credit to them if I took up a PhD on the top of the world. And it is with the support of the Knut and Alice Wallenberg Foundation, the Swedish Research Council and the European Community Framework Programme 7 EuCARD , through Tord Ekelöf, that I have been accepted as a PhD student at Uppsala University. Nevertheless, it is thanks to my supervisor, Volker, if I have finally got to this point, and to whom goes my sincere gratitude for his guidance and passionate dedication helping me to get things done and achieving my goals.

During these five years as a PhD student at Uppsala University I travelled a lot, much more that I could possibly ask for. A considerable amount of these travels brought me to CERN, where I spent almost one year in bit and peaces, trying to make my way through a jungle of people, tasks and ideas. There, I could always count on the cautious and constant support of my supervisor, Roger, who always negotiated beam time trying to save me from long nights of data taking.

I can't but express my gratitude to all those who shared their time and expertise with me, discussing and helping me developing what has finally turned into this thesis. Most of all, to Wilfrid goes all my gratitude for the invaluable support at work and not only. I am glad we met and shared a big part of the work of these years.

Luckily, my staying at CERN has never meant only work. I cannot imagine surviving there without the priceless presence of Davide, Luca and Simona. Your professional help is indisputable, and I will never forget the nights spent together in the control room trying to make that machine run, but most of all you guys made my time there much happier.

On top of that, crossing the path of old friends that were at CERN when I was also there was invaluable. Michelangelo, Sarita, Flavio and Valentina, knowing that you where there has always been reassuring.

And now back to Uppsala, where I spent most of my time. Maja, it has been awesome to share the joy and pain of this last year of PhD

together! Marek, thanks for being always ready to help and to patiently listen to my complaints (note that I am very good at that). Tomoko - I still remember the first cold winter day when you visited us - thanks for your always friendly support. Not to mention Stephan, first friend at Uppsala University, and Jim, Gergana, Rocio, Mathias, Niklas, Masih and all the other colleagues and fellow students that I met here.

But this is just the beginning, cause the number of people that crossed my path and with whom I shared my everyday life during this five years is large, and all of them deserve a very special thank. Riccardo, my first and most precious friend here in Sweden. Paolo and Moreno, among the first of that which has become a pretty numerous Italian crew in Uppsala with my favourite teacher Tony, who brought me back to singing, Luca, my favourite break buddy, Arianna, Valentina, Chiara, Lorenzo, Diego, Giuseppe, Matteo, Marco, Cecilia, Valeria e Johan. And Liliana, Hannah and Blaize, best roommates ever!

The past year has been full of changes, accompanied by new unexpected friends: Umberto, Elisabetta, Sebastian and Frida. And a special thank goes to Rob and Ana, everything would be so much greyer without you guys!

Not everyone was close though, but it was as if they were here. Mom and dad, thanks for your absolute support and for trying to avoid to show that you would like to have me there. And my brothers, Guido and Lorenzo, what would I do without you? And then, of course, there are all my lifelong friends, those who I know will always be there, no matter how far we are of how long it is since last time that we met: Vincenzo, Annalisa, Manuela, Caterina, Valerio, Annalisa, Michela, Fabrizio e Alessandro.

Finally, I did not comment on the remaining chunk of trips that did not bring me to CERN. Well, those brought me to Berlin where Sara has always been waiting for me. Despite the distance, you have always managed to be by my side, to share each and every moment of the last five years, whose memories will be inextricably linked to you.

Summary in Swedish

Vår nuvarande förståelse av materiens grundläggande beståndsdelar och de fundamentala krafter som styr deras interaktioner beskrivs inom partikelfysiken av den så kallade Standardmodellen. Det är en teori som har visat sig vara giltig över ett brett spektrum av energier och har klarat ett stort antal stränga tester. Dock är många frågor inom partikelfysiken ännu osvarade och de kräver att forskningen om partiklar utvidgas.

Detta sker till exempel i experiment vid partikelkrossare, bland vilka kan nämnas Large Hadron Collider vid CERN, där den länge eftersökta Higgs-bosonen nyligen observerades. För att bekräfta en sådan upptäckt och för att fortsätta sökandet efter ny fysik, behövs en maskin som kan kollidera partiklar med ännu högre energi. CLIC, vilket står för Compact Linear Collider, är en kandidat till en sådan anläggning och utgör ett stort forskningsprojekt.

Jämfört med alla partikelacceleratorer som byggts hittills, är CLIC baserad på en helt ny teknik, vilken har utvecklats för att hålla projektet inom en rimlig kostnad och storlek. Den består av att partiklarna accelereras med en stor gradient med hjälp av starka elektriska fält som genererats av en annan partikelstråle. Sådana höga fältstyrkor innebär en högre risk för vakuumurladdningar, ett fenomen känt sedan mer än ett sekel men vars mikroskopiska natur ännu inte är helt klarlagd. Känt är dock att en vakuumurladdning i acceleratorn kan påverka partikelstrålen och leda till en allvarlig försämring av partikelkrossarens prestanda. Förståelsen av fysiken bakom vakuumurladdning i accelerationsstrukturer och dess inverkan på partikelstrålen har därför blivit en viktig fråga för utformningen av en pålitlig accelerator baserad på CLIC-teknik.

Denna avhandling beskriver experimentella studier som behandlar detta problem.

Ett första experiment genomfördes vid Stanford National Acelerator Laboratory i USA och omfattade tester på en prototyp för en accelerationsstruktur för CLIC. I denna typ av experiment studeras prestandan hos accelerationsstrukturer då de är anslutna till en konventionell källa för radiofrekvensstrålning. I vårt experiment var strukturen som skulle testas monterad i en så kallad resonansring, vilken fungerar som en förstärkare och används för att öka fältstyrkan i strukturen. Vi beskriver detta experiment med hjälp av en matematisk modell, på vilken vi också har baserat en metod för att karakterisera plasma som bildas under

en urladdning. Dessutom visade vi att det är möjligt att beräkna var i accelerationsstrukturen som individuella urladdningar sker, baserat på mätningar av radiofrekvensstrålningens styrka och fas.

Delar av den matematiska modellen utgjorde grunden för studier av effekterna av urladdningar på en partikelstråle. Dessa tester utfördes vid Two-beam Test Stand, en experimentuppställning som Uppsala universitet byggt vid testanläggningen för CLIC, CTF3, på det internationella laboratoriet för partikelfysik CERN. Där testade vi en accelerationsstruktur av CLIC-typ med en elektronstråle. Vi fann att urladdningar kan påverka både den längsgående och den tvärgående rörelsemängden hos partikelstrålen, vilket orsakar en minskning av accelerationsgraden samt avlänkningar av partikelstrålbanan.

Eftersom de kolliderande partikelstrålarna i CLIC måste kontrolleras ner till en aldrig tidigare skådad noggrannhet på nanometernivå är våra resultat viktiga för utformningen av CLIC. Slutligen diskuterar vi därför effekten av våra resultat för CLIC och dess prestanda.

Summary in Italian

La nostra attuale conoscenza dei costituenti fondamentali della materia e delle forze che governano le loro interazioni è descritta dal Modello Standard della fisica delle particelle, una teoria che ha dimostrato di essere valida in un ampio intervallo di energie e in un vasto numero di prove sperimentali. Nonostante ciò sono molte le domande che ancora non trovano risposta ed è per cercare di rispondere a queste che è necessario estendere ulteriormente la ricerca di base in questo campo.

Questo tipo di ricerca viene portata avanti in esperimenti presso collisori di particelle, tra i quali è bene ricordare il Large Hadron Collider al CERN, dove recentemente è stato finalmente osservato il tanto cercato bosone di Higgs. Per confermare questa scoperta e per continuare la ricerca di nuova fisica, è necessaria una macchina capace di far collidere particelle ad un'energia ancora maggiore e il Compact Linear Collider, CLIC, è un progetto che risponde a tale esigenza.

A differenza di tutti gli acceleratori costruiti fino ad ora, CLIC è basato su una nuova tecnica di accelerazione, sviluppata ad hoc per contenere i costi e le dimensioni del progetto. La sua peculiarità risiede nel fatto che fasci di particelle sono accelerati con un alto gradiente utilizzando intensi campi elettrici prodotti con un altro fascio di particelle in un secondo acceleratore. L'uso di campi elettrici così intensi però comporta il verificarsi di scariche nelle strutture acceleratrici, un fenomeno conosciuto da oltre un secolo la cui dinamica microscopica non è stata però ancora completamente compresa e il cui impatto sul fascio di particelle che viene accelerato può provocare una seria riduzione delle prestazioni del collisore. La comprensione della fisica alla base di questo fenomeno e del suo impatto sul fascio di particelle accelerato è perciò diventato un argomento di primo piano nel contesto dello studio di un collisore di particelle basato sulla tecnologia di CLIC.

Questa tesi tratta di esperimenti mirati a investigare questo argomento.

Un primo esperimento riguarda il test di un prototipo di struttura acceleratrice di CLIC, condotto presso il Stanford National Acelerator Laboratory. In questo genere di esperimenti, strutture acceleratrici vengono alimentate con sorgenti convenzionali di radiofrequenze per studiare le loro prestazioni. Nel nostro esperimento la struttura in esame era assemblata in un anello risonante, una sorta di amplificatore utilizzato per aumentare la potenza nella struttura. Questo esperimento è stato

caratterizzato con un modello matematico, sulla base del quale abbiamo proposto un metodo per caratterizzare il plasma che si forma durante un scarica. Inoltre, abbiamo dimostrato che è possibile stimare dove single scariche avvengono nella struttura sotto esame sulla base di misure di potenza e fase della radiofrequenza.

La stessa metodologia pone le basi per lo studio dell'impatto che queste scariche hanno sul fascio di particelle che viene accelerato. Tale studio è stato portato avanti al Two-beam Test Stand, un'area sperimentale costruita dall'Università di Uppsala presso il complesso sperimentale di CLIC, CTF3, nel laboratorio internazionale di fisica delle particelle CERN. In quel contesto abbiamo testato un prototipo di struttura acceleratrice per CLIC in presenza di un fascio di elettroni e abbiamo osservato che le scariche in esame possono avere un effetto sia sulla quantità di moto longitudinale che su quella trasversale del fascio, causando una riduzione del gradiente con cui questo viene accelerato oltre a una deviazione della traiettoria delle particelle.

Dal momento che i fasci di particelle che collidono in CLIC devono essere allineati con una precisione a livello nanometrico mai raggiunta prima, abbiamo riscontrato che effetti come quelli osservati possono avere una rilevanza notevole sulle sue prestazioni.

References

[1] S. L. Glashow. Partial-symmetries of weak interactions. *Nuclear Physics*, 22(4):579–588, 1961.

[2] S. Weinberg. A model of leptons. *Phys. Rev. Lett.*, 19:1264–1266, Nov 1967.

[3] A. Salam and J. Ward. Weak and electromagnetic interactions. *Il Nuovo Cimento Series 10*, 11(4):568–577, 1959.

[4] G. 't Hooft and M. Veltman. Regularization and renormalization of gauge fields. *Nuclear Physics B*, 44(1):189 – 213, 1972.

[5] P. W. Higgs. Broken symmetries and the masses of gauge bosons. *Phys. Rev. Lett.*, 13:508–509, Oct 1964.

[6] P. W. Higgs. Spontaneous symmetry breakdown without massless bosons. *Phys. Rev.*, 145:1156–1163, May 1966.

[7] F. Englert and R. Brout. Broken symmetry and the mass of gauge vector mesons. *Phys. Rev. Lett.*, 13:321–323, Aug 1964.

[8] J. R. Ellis. Supersymmetry for Alp Hikers. page 45 p, Mar 2002, hep-ph/0203114.

[9] G. Arnison, A. Astbury, B. Aubert, et al. Experimental observation of isolated large transverse energy electrons with associated missing energy at $\sqrt{s}$=540 GeV. *Physics Letters B*, 122(1):103–116, 1983.

[10] G. Arnison, A. Astbury, B. Aubert, et al. Experimental observation of lepton pairs of invariant mass around 95 GeV/c^2 at the CERN SPS collider. *Physics Letters B*, 126(5):398–410, 1983.

[11] P. Bagnaia, M. Banner, R. Battiston, et al. Evidence for $z^0 \to e^+e^-$ at the CERN $\overline{p}p$ collider. *Physics Letters B*, 129(1-2):130–140, 1983.

[12] F. Abe, H. Akimoto, A. Akopian, et al. Observation of top quark production in $\overline{p}p$ collisions with the collider detector at Fermilab. *Phys. Rev. Lett.*, 74:2626–2631, Apr 1995.

[13] ATLAS collaboration. Observation of a new particle in the search for the standard model higgs boson with the ATLAS detector at the LHC. *Physics Letters B*, 716(1):1–29, 2012.

[14] CMS collaboration. Observation of a new boson at a mass of 125 GeV with the CMS experiment at the LHC. *Physics Letters B*, 716(1):30–61, 2012.

[15] T. Behnke, J. E. Brau, B. Foster, et al. The international linear collider technical design report - volume 1: Executive summary, 2013, arXiv:1306.6327.

[16] M. Aicheler, P. Burrows, M. Draper, et al. A multi-TeV linear collider based on CLIC technology: CLIC Conceptual Design Report. Technical Report CERN-2012-007, SLAC-R-985, KEK-Report-2012-1, PSI-12-01, JAI-2012-001, CERN, Geneva, 2012.

[17] C. Adolphsen, M. Barone, B. Barish, et al. The international linear collider technical design report - volume 3.ii: Accelerator baseline design, 2013, arXiv:1306.6328.
[18] C. Adolphsen, M. Barone, B. Barish, et al. The international linear collider technical design report - volume 3.i: Accelerator r&d in the technical design phase, 2013, arXiv:1306.6353.
[19] P. Lebrun, L. Linssen, A. Lucaci-Timoce, et al. The CLIC programme: towards a staged e^+e^- linear collider exploring the terascale. Technical report, CERN, 2012, 1209.2543.
[20] The seventy-first session of the CERN council : Lep project given the go-ahead, 1981. Issued on 17 December 1981.
[21] CERN. *ECFA-CERN Workshop on Large Hadron Collider in the LEP Tunnel*, number CERN-84-10-V-1; ECFA-84-085-V-1, Geneva, May 1984. CERN.
[22] The Large Hadron Collider Project (Resolution Annex 1+2). Le projet du grand collisionneur de hadrons. 100th Session of Council, Jun 1994.
[23] J. D. Lawson. Linear collider constraints: some implications for future accelerators. Technical report, CERN, 1985.
[24] A. M. Sessler. The free electron laser as a power source for a high-gradient accelerating structure. *AIP Conference Proceedings*, 91(1):154–159, 1982.
[25] A. M. Sessler and S. S. Yu. Relativistic klystron two-beam accelerator. *Phys. Rev. Lett.*, 58:2439–2442, Jun 1987.
[26] Y. Honda, K. Kubo, S. Anderson, et al. Achievement of ultralow emittance beam in the accelerator test facility damping ring. *Phys. Rev. Lett.*, 92:054802, Feb 2004.
[27] M. Aiba, M. Böge, N. Milas, and A. Streun. Ultra low vertical emittance at SLS through systematic and random optimization. *Nuclear Instruments and Methods in Physics Research Section A: Accelerators, Spectrometers, Detectors and Associated Equipment*, 694(0):133–139, 2012.
[28] Detailed Design Report on the MAX IV facility. Technical report, MAX-lab, Aug 2010.
[29] R. Hettel, K. Bane, L. Bentson, et al. Ideas for a future PEP-X light source. *Proceedings of EPAC08, Genoa, Italy*, C0806233:WEPC023, 2008.
[30] Y. Baconnier, K. K. Geissler, K. Hübner, and J. H. B. Madsen. A CLIC injector test facility. Technical Report CLIC-Note-65, CERN, Geneva, Jun 1998.
[31] H. H. Braun. Experimental Results and Technical Results and Development at CTFII. In *Proceedings of EPAC2000, Vienna, Austria*, June 2000.
[32] I. H. Wilson. Proposals for future CLIC studies and a new CLIC Test Facility (CTF3). Technical Report CERN-PS-99-047-LP. CLIC-Note-402, CERN, Geneva, Jul 1999.
[33] H. Braun, J. P. Delahaye, G. Geschonke, et al. R and D for the feasibility study of CLIC technology. Technical report, CERN, Aug 2004.

[34] R. L. Lillestøl, S. Döbert, M. Olvegård, and E. Adli. Experimental results from the test beam line in the CLIC test facility 3. Technical Report CERN-ACC-2013-0207, CERN, Geneva, May 2013.
[35] A. Mosnier, M. Authier, A. Bogard, D. andCurtoni, et al. The probe beam linac in CTF3. In *Proceedings of EPAC 2006, Edinburgh, Scotland*, pages 679–681, 2006.
[36] V. Ziemann, H.-H. Braun, S. Doebert, et al. The two-beam test-stand in CTF3. In *Proceedings of EPAC 2006, Edinburgh, Scotland*, pages 2445–24447, 2006.
[37] M. Gasior. An inductive pick-up for beam position and current measurements. In *6th European Workshop on Beam Diagnostics and Instrumentation for Particle Accelerators, Mainz, Germany*, pages 53–56, 2003.
[38] C. Simon, D. Bogard, and M. Luong. Instrumentation for high frequency cavity BPM in CALIFES. In *Proceedings of PAC09, Vancouver, BC, Canada*, pages 3497–3499, 2009.
[39] W. Farabolini, G. Adroit, P. Girardot, et al. Video Profile Monitors Development for the CTF3 Probe Beam Linac. In *Proceedings of EPAC08, Genoa, Italy*, pages 1101–1103, 2008.
[40] CERN Drawing Database. `http://edms-service.web.cern.ch/edms-service/CDD/`.
[41] R. Latham. *High voltage vacuum insulation: the physical basis*. Academic Press, 1981.
[42] R. H. Fowler and L. Nordheim. Electron emission in intense electric fields. In *Proceedings of the Royal Society of London. Series A, Containing Papers of a Mathematical and Physical Character*, volume 119, pages 173–181. Proc. R. Soc. Lond. A, May 1928.
[43] N. Ashcroft and N. Mermin. *Solid state physics*. Saunders College, 1976.
[44] J. W. Kovermann. *Comparative Studies of High-Gradient Rf and Dc Breakdowns*. PhD thesis, Aachen, Tech. Hochsch., Aachen, 2010. Presented 17 Dec 2010.
[45] S. Dobert, C. Adolphsen, G. Bowden, et al. High gradient performance of NLC/GLC X-band accelerating structures. In *Particle Accelerator Conference, 2005. PAC 2005. Proceedings of the*, pages 372–374, 2005.
[46] A. Grudiev, S. Calatroni, and W. Wuensch. New local field quantity describing the high gradient limit of accelerating structures. *Phys. Rev. ST Accel. Beams*, 12:102001, Oct 2009.
[47] T. Muranaka, T. Blom, K. Leifer, and V. Ziemann. Instrumental developments for in situ breakdown experiments inside a scanning electron microscope. *Nuclear Instruments and Methods in Physics Research Section A: Accelerators, Spectrometers, Detectors and Associated Equipment*, 657(1):122–125, 2011.
[48] E. IFEACHOR and B. JERVIS. *Digital Signal Processing: A Practical Approach*. Electronic Systems Engineering Series. Addison-Wesley, 1993.
[49] W. Press. *Numerical Recipes with Source Code CD-ROM 3rd Edition: The Art of Scientific Computing*. Cambridge University Press, 2007.

[50] V. A. Dolgashev and T. Raubenheimer. Simulation of RF breakdown effects on NLC beam. In *22nd International Linear Accelerator Conference, Lubeck, Germany*, pages 396–398, August 2004.
[51] V. A. Dolgashev, K. L. F. Bane, G. Stupakov, J. Wu, and T. O. Raubenheimer. Effect of dark currents on the accelerated beam in an X-band linac. In *Proceedings of EPAC 2004, Lucerne, Switzerland*, pages 2203–2205, 2004.
[52] C. Adolphsen. Advances in normal conducting accelerator technology from the X-band linear collider program. In *Proceedings of 2005 Particle Accelerator Conference, Knoxville, Tennessee*, number SLAC-PUB-11224, pages 204 – 208. IEEE, Jun 2005.
[53] M. Johnson. Beam-based diagnostics of RF-breakdown in the Two-Beam Test-Stand in CTF3. Technical Report CERN-OPEN-2007-022. CLIC-Note-710, CERN, Geneva, Aug 2007. revised version submitted on 2007-09-28 15:15:42.
[54] C. Simon, M. Luong, S. Chel, et al. Performance of a reentrant cavity beam position monitor. *Phys. Rev. ST Accel. Beams*, 11:082802, Aug 2008.
[55] A. Grudiev, A. Latina, and D. Schulte. Study of Fundamental Mode Multipolar Kicks in Double- and Single-feed Power Couplers for the CLIC Main Linac Accelerating Structure. In *Proceedings of IPAC2012, New orleans, Louisiana, USA*, pages 3081–3083, 2012.
[56] W. Fischer. *An experimental study on the long-term stability of particle motion in hadron storage rings*. PhD thesis, Universität Hamburg, Hamburg, 1995.
[57] F. Decker, C. Adolphsen, W. Corbett, et al. Dispersion and betatron matching into the linac. In *Proceedings of Particle Accelerator Conference, San Francisco, USA*, volume 2, pages 905–907, 1991.
[58] J. Jackson. *Classical Electrodynamics*. Wiley, 1998.
[59] S. Lee. *Accelerator Physics*. World Scientific, 2004.
[60] R. Q. Twiss and N. H. Frank. Orbital Stability in a Proton Synchrotron. *Review of Scientific Instruments*, 20(1), 1949.
[61] E. D. Courant and H. S. Snyder. Theory of the alternating-gradient synchrotron. *Annals of Physics*, 3(1):1–48, 1958.
[62] A. Chao. *Handbook of Accelerator Physics and Engineering*. World Scientific, 1999.
[63] D. Pozar. *Microwave engineering*. Wiley, 1997.
[64] T. Wangler. *RF Linear Accelerators*. Physics Textbook. Wiley, 2008.

Appendix A. Fundamentals of beam physics

Beam physics deals with the description of the motion of ensembles of charged particles, or beams, in an accelerator. An accelerator, in turn, can be thought of as a periodic sequence of electromagnetic fields, so-called lattice, that constrain a beam to a well defined path called reference trajectory, which is the ideal trajectory of a reference particle with a given energy. Along this path, all the particles in the beam are guided, accelerated and in some cases collided onto a target.

The description of the dynamics of charged particles in electromagnetic fields is thoroughly discussed in many books, such as Ref. [58]. What motivates this digression on beam physics is rather the intention to offer a review of the concepts used in this thesis to describe experimental observations and the context in which they were carried out.

A convenient framework to describe the motion of a charged particle in an electromagnetic field is the Hamiltonian formalism, which is also the approach followed in Ref. [59]. That has the advantage of providing a robust way of deriving the equations of motion through the Hamilton-Jacobi equations. Moreover, its symplectic structure ensures that phase space coordinates are mapped into coordinates of the same phase space whose temporal evolution is described by the same equations of motion.

A particle in an accelerator is uniquely defined by six canonical variables, i.e. its coordinates and momenta, thus by a point in a 6-dimensional phase space. Its motion is conveniently described in a curvilinear reference frame like the one shown in Fig. 8.1, where no torsion is assumed. Often the curvilinear coordinate is used in place of time as independent variable, in which case the arrival time τ and the energy deviation δ with respect to the reference particle are used in place of the longitudinal coordinate and momentum. That is also the description followed hereafter. Once the Hamiltonian and the electromagnetic field are expressed accordingly, the equations of motion can be derived which map any particle coordinates between two points in the lattice.

The simplest case is that of a *drift* space of length L, i.e. empty space in which there is no electromagnetic field, where the motion of a charged particle is uniform rectilinear. If we consider the motion limited to a couple of conjugate variables, say the horizontal coordinate x and its derivative with respect to the curvilinear abscissa $x' = \frac{dx}{ds}$, the coefficients of the solutions of the equations of motion can be written in terms of a matrix, so-called *transfer matrix*, such that the beam coordinates

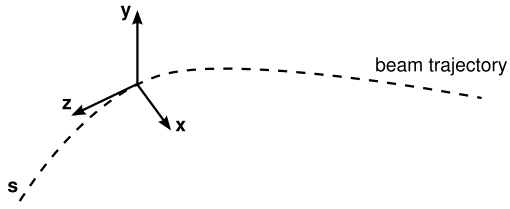

Figure 8.1: Curvilinear reference system.

(x_0, x_0') at the beginning of the drift space are transformed into the final coordinates (x, x') at the end of the drift space as follows:

$$\begin{pmatrix} x \\ x' \end{pmatrix} = \begin{pmatrix} 1 & L \\ 0 & 1 \end{pmatrix} \begin{pmatrix} x_0 \\ x_0' \end{pmatrix} \tag{8.1}$$

If the dynamics is uncoupled in the transverse plane, the two-by-two matrix that describes the motion in one of the transverse dimensions describes it also in the other one. Moreover, the transfer matrix formalism can be extended to all canonical variables so that any phase space coordinate at any curvilinear abscissa is expressed by a linear combination of all the phase space coordinates at any upstream abscissa through a six-dimensional square matrix that represents that particular section of the beam line.

The same way of reasoning is applied to describe the motion through an electromagnetic field of length L. If the field is quadrupolar, it acts like an optical lens which focuses in one plane and defocuses in the other. The motion in this case is non-linear but a linear map can be derived by expanding the Hamiltonian in the dynamic variables, or equivalently the equations of motions or their solutions, under the assumption that the motion is close to that of the reference particle. The transfer matrix which describes the motion in the focusing plane is

$$R_{FQ} = \begin{pmatrix} \cos\left(\sqrt{k}l\right) & \sin\left(\sqrt{k}l\right)/\sqrt{k} \\ -\sqrt{k}\sin\left(\sqrt{k}l\right) & \cos\left(\sqrt{k}l\right) \end{pmatrix} \tag{8.2}$$

whereas the defocusing effect is described on the other plane by the matrix

$$R_{DQ} = \begin{pmatrix} \cosh\left(\sqrt{k}l\right) & \sinh\left(\sqrt{k}l\right)/\sqrt{k} \\ \sqrt{k}\sinh\left(\sqrt{k}l\right) & \cosh\left(\sqrt{k}l\right) \end{pmatrix}. \tag{8.3}$$

The complete transfer matrix for a quadrupole is therefore

$$R_Q = \begin{pmatrix} R_{FQ} & 0 & 0 & 0 \\ 0 & R_{DQ} & 0 & 0 \\ 0 & 0 & 1 & \frac{L}{\beta^2\gamma^2} \\ 0 & 0 & 0 & 1 \end{pmatrix} \tag{8.4}$$

where the element $(R_Q)_{56}$ describes the fact that a particle with an energy deviation δ with respect to the energy of the reference particle, arrives with a delay $\tau = \frac{L}{\beta^2\gamma^2}$. In some cases, the length of the field can be neglected and in such case, called thin lens approximation, under the assumption that $L \to 0$, the transfer matrix in the transverse plane is

$$R_Q^{(thin)} = \begin{pmatrix} 1 & 0 \\ \mp\frac{1}{f} & 1 \end{pmatrix} \tag{8.5}$$

where f is the focal length and the sign $\mp$ corresponds to the focusing and defocusing plane, respectively.

The transfer matrix of a portion of beam line which contains different elements, is derived by multiplying the transfer matrices of all such elements in the order seen by the beam. As an example, we derive here the transfer matrix of a lattice consisting of a thin focusing quadrupole, a drift space and a thin defocusing quadrupole. This configuration is called FODO lattice and it is shown in Fig. 8.2. Its transfer matrix R is

$$R = R_D(\tfrac{L}{2}) \cdot R_{FQ}^{(thin)} \cdot R_D(L) \cdot R_{DQ}^{(thin)} \cdot R_D(\tfrac{L}{2}) \tag{8.6}$$

where $R_D(L)$ denotes the transfer matrix of a drift space of length L.

The way a transfer matrix is defined ensures that it is symplectic, and has therefore unit determinant. Hence, a two-by-two transfer matrix can be parametrised by three coefficients, which in this context are commonly known as Twiss parameters [60] or Courant-Snyder parameters [61]. Their values are a function of the curvilinear abscissa, i.e. they

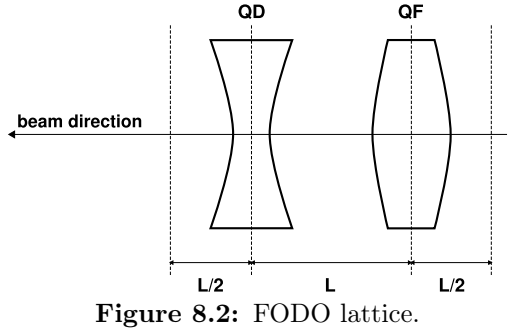

Figure 8.2: FODO lattice.

assume different values along the beam line. Moreover, they are related to the semi-axes of the ellipse spanned by a particle in the phase space.

Now that we have recalled the basics of the description of the motion of a charged particle between two points in the beam lattice, we extend it to the more realistic case of an ensemble of particles, whose trajectories are close to that of the reference particle. Each particle of such ensemble is described by a point in the phase space and altogether such points occupy a volume that is called *emittance* of the beam, which is invariant during the motion of the particles in the beam lattice. In the phase space of a couple of conjugate variables, the emittance is proportional to the area of an ellipse, whose shape is described by the Twiss parameters.

The macroscopic characteristics of an ensemble of particles, the beam, are conveniently described in terms of its statistical properties. These are the statistical moments of the distributions of the six canonical variables. The first order moments are the three mean positions and momenta of the beam. The first three describes the barycentre of the beam and their motion lies in the proximity of the reference trajectory. The second order moments are the standard deviations of the distributions of positions and momenta, i.e. the beam sizes and divergences, and their correlations. These 21 parameters are commonly represented with the covariance matrix, which in this context is called beam matrix σ and characterises the beam at any point along the beam line. In the horizontal plane, it is

$$\sigma = \begin{pmatrix} \langle x^2 \rangle & \langle x' \rangle \\ \langle x' \rangle & \langle x'^2 \rangle \end{pmatrix}. \tag{8.7}$$

The beam matrix is mapped to any point in the beam line in the same way described for the case of a single particle, through

$$\sigma = R\sigma_0 R^T \tag{8.8}$$

where σ_0 is the initial beam matrix and R is the transfer matrix between any two points of the beam lattice. If we take the determinant of both members of Eq. 8.8 and we use the fact that the transfer matrix R is symplectic and that therefore it has unit determinant, we find that the determinant of the beam matrix is conserved. That is proportional to the beam emittance. Similarly to the case of a transfer matrix, the beam matrix can also be parametrised in terms of the Twiss parameters α, β and γ, as follows:

$$\sigma = \epsilon \begin{pmatrix} \beta & -\alpha \\ -\alpha & \gamma \end{pmatrix} \tag{8.9}$$

where ϵ is the beam emittance.

Luminosity

The ultimate goal in a particle collider is to actually collide particles so that the physics of the collisions and of their outcome can be studied. Because such physics is described by quantum mechanics, the number of actual collisions at the point where particles interact depends on a certain probability, specific for any given process, called *cross-section*. The proportionality factor $\mathcal{L}$ between the cross-section σ and the number N of interactions per second in a collider is called *luminosity*:

$$\frac{dN}{dt} = \mathcal{L}\sigma_p \tag{8.10}$$

and is traditionally expressed in $\mathrm{cm}^{-2}\,\mathrm{s}^{-1}$ in the CGS system of units.

A beam of particles impinges on a target at the interaction point. In the case of a collider the target is represented by another beam and the luminosity is defined as the 4-dimensional overlap integral of the two colliding charge distributions $\rho_\pm$ in space and time travelling with velocity $\vec{v}_\pm$ [62, chap. 4.1]:

$$\mathcal{L}_{sc} = \frac{1}{c}\int d^3x dt \rho_+(\vec{x},t)\rho_-(\vec{x},t)\sqrt{c^2(\vec{v}_+ - \vec{v}_-)^2 - (\vec{v}_+ \times \vec{v}_-)^2} \tag{8.11}$$

where the factor under the square root symbol is the kinematic factor K which becomes $K = 2c^2$ in case of ultra-relativistic beams that collide head-on. In that case the luminosity is

$$\mathcal{L}_{sc} = 2c\int d^3x dt \rho_+(\vec{x},t)\rho_-(\vec{x},t) \tag{8.12}$$

whereas in case of a fixed target experiment where a relativistic beam impinges on a target at rest, the kinematic factor is $K = c^2$ and the luminosity is only half of the luminosity of two colliding beams.

The luminosity defined so far is called single-collision luminosity. In a storage ring collider, with bunch spacing s_B, bunches collide periodically with a frequency $f_c = \beta c/s_B$. In a linear collider, the collision frequency is the product of the repetition rate and the number of bunches per bunch-train. The product of the single-collision luminosity and the collision frequency is called peak luminosity.

Now let's have a look at the charge density distributions $\rho_\pm$. One example is the case of no coupling between transverse and longitudinal coordinates, in which case the charge density distribution can be written as

$$\rho_\pm(x,y,s,t) = \rho_\pm(x)\rho_\pm(x)\rho_\pm(s \mp s_0) \tag{8.13}$$

where s is the longitudinal coordinate and $s_0 = ct$ is the distance of a relativistic bunch from the interaction point $s = 0$ at the time t. The

luminosity is therefore:

$$\mathcal{L} = f_c \mathcal{L}_{sc} = 2 f_c \int d^3x ds_0 \rho_{\pm}(x) \rho_{\pm}(x) \rho_{\pm}(s \mp s_0) \tag{8.14}$$

The analytic solution of the latter integral depends on the explicit form of the charge density distributions $\rho_{\pm}$. In the case of Gaussian distributions with standard deviations σ_x, σ_y and σ_s in the horizontal, vertical and longitudinal plane, respectively, Eq. 8.14 has the solution

$$\mathcal{L} = \frac{N_+ N_- f_c}{4\pi \sigma_x \sigma_y} \tag{8.15}$$

where we assumed identical charge density distribution for the two colliding beams.

Appendix B. Fundamentals of rf technology

In this appendix we briefly describe the rf components, waveguides and resonant structures, that are used in an accelerator to transport power and accelerate charged particles. This topics is thoroughly discussed in many books, both from a purely physical point of view as in Ref. [58], and with a more technical approach applied to microwave engineering [63] or linear particle accelerators [64]. Therefore this digression is limited to a general description of the concepts used in this thesis.

The dynamics and properties of electromagnetic fields are described by Maxwell's equations. These are a set of partial differential equations which, in absence of charges and currents assume the form of a hyperbolic partial differential equation known as d'Alembert equation or wave equation. Its specific solution depends on the particular choice of boundary conditions which, in the case at hand, are defined by the geometry of a waveguide or of an accelerator structure.

The solution of the wave equation can be written as a superposition of Fourier components, each one corresponding to a specific pattern of electric magnetic fields which is called *propagation mode*. If the longitudinal component of the magnetic field is zero the mode is called *transverse magnetic* (TM), whereas if the longitudinal component of the electric field is zero the mode is called *transverse electric* (TE). Transverse modes are labelled with two indices, according the number of half-wavelengths across the dimensions of the waveguide. Moreover, to each propagation mode corresponds a cutoff frequency, i.e. the minimum frequency with which that mode can propagate without attenuation. The mode with the lowest cutoff frequency is called dominant or fundamental mode.

When the boundary conditions are defined by the geometry of a rectangular waveguide, the lowest cutoff frequency occurs for the TE_{10} mode. When the boundary conditions are defined by the geometry of a cylindrical waveguide, the lowest cutoff frequency occurs for the TE_{11} mode.

While a waveguide is a very convenient way of transporting power, it is not as convenient when it comes to transferring such power to a charged particle. For that, two conditions must be met: first, the field must have an electric component along the direction of motion of the particle. Second, the particle must match the velocity at which the field propagates, so-called *phase velocity*, in order to be continuously accelerated. The first condition can be satisfied, for instance, by transverse magnetic propagation modes in a waveguide, whereas the second condition is never satisfied in a waveguide since the phase velocity there

is bigger than the speed of light. A way to get around it is to confine the field in a section of waveguide by terminating both its ends with conductive surfaces. This way the field bounces back and forth between the two end walls creating a stationary pattern or standing wave, hence this device is called standing-wave cavity. If the length of the cavity is a multiple integer of the field wavelength it is said to resonate and the amplitude of the stationary field pattern is maximised.

A second approach is to propagate an electromagnetic field in a waveguide-like structure where "obstacles" are placed in order to slow down the field. This geometry, sketched in Fig. 8.3, is basically a periodic array of coupled standing-wave cavities or cells. The "obstacles", or loads, are typically disks with a small aperture that lets the field leak through and propagate to the next cell. This device is called travelling-wave disk-loaded cavity because the field propagates through it until it reaches the output port where it is generally dumped in a load. In this type of cavities, the field has a different phase in each cell, and the phase difference between two adjacent cells is called phase advance.

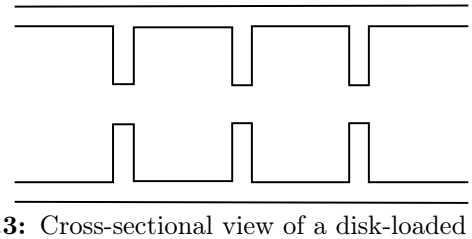

Figure 8.3: Cross-sectional view of a disk-loaded waveguide.

In a resonant cavity the propagation modes of the field are labelled similarly to the case of waveguides, with the addition of a third index that takes into account the length of the cavity. A standard acceleration mode in a circular cavity is the TM_{010}, that has a longitudinal electric field on the axis of the cavity which accelerates the particles.

So far we have neglected the fact that both waveguides and resonant cavities are made of conductive materials, whose finite conductivity is the source of power dissipation by Joule effect. In other words, the electromagnetic field gradually looses energy while it propagates and therefore the strength of the field along the structure decreases. The ratio between the power delivered to the beam and the power dissipated in the structure is called *beam-loading* ratio [64, see chap. 2.5]. In case a constant gradient has to be maintained, the aperture of the disks can be tapered along the structure in such a way that the velocity at which the energy propagates in the structure, i.e. the group velocity of the field, decreases and the gradient remains constant. That is the choice for the CLIC accelerator structures design.

Acta Universitatis Upsaliensis

Digital Comprehensive Summaries of Uppsala Dissertations from the Faculty of Science and Technology 1096

Editor: The Dean of the Faculty of Science and Technology

A doctoral dissertation from the Faculty of Science and Technology, Uppsala University, is usually a summary of a number of papers. A few copies of the complete dissertation are kept at major Swedish research libraries, while the summary alone is distributed internationally through the series Digital Comprehensive Summaries of Uppsala Dissertations from the Faculty of Science and Technology.

Distribution: publications.uu.se
urn:nbn:se:uu:diva-208567

ACTA
UNIVERSITATIS
UPSALIENSIS
UPPSALA
2013